

---

# LSALSA: efficient sparse coding in single and multiple dictionary settings

---

Benjamin Cowen  
 Apoorva Nandini Saridena  
 Anna Choromanska

BC1947@NYU.EDU  
 ANS609@NYU.EDU  
 AC5455@NYU.EDU

## Abstract

We propose an efficient sparse coding (SC) framework for obtaining sparse representation of data. The proposed framework is very general and applies to both the single dictionary setting, where each data point is represented as a sparse combination of the columns of one dictionary matrix, as well as the multiple dictionary setting as given in morphological component analysis (MCA), where the goal is to separate the data into additive parts such that each part has distinct sparse representation within an appropriately chosen corresponding dictionary. Both tasks have been cast as  $\ell_1$ -regularized optimization problems of minimizing quadratic reconstruction error. In an effort to accelerate traditional acquisition of sparse codes, we propose a deep learning architecture that constitutes a trainable time-unfolded version of the Split Augmented Lagrangian Shrinkage Algorithm (SALSA), a special case of the alternating direction method of multipliers (ADMM). We empirically validate both variants of the algorithm on image vision tasks and demonstrate that at inference our networks achieve improvements in terms of the running time and the quality of estimated sparse codes on both classic SC and MCA problems over more common baselines. We finally demonstrate the visual advantage of our technique on the task of source separation.

## 1. Introduction

In the SC framework, we seek to efficiently represent data by using only a sparse combination of available basis vectors. We therefore assume that an  $M$ -dimensional data vector  $\mathbf{y} \in \mathbb{R}^M$  can be approximated as

$$\mathbf{y} \approx \mathbf{A} \mathbf{x}^*, \quad (1)$$

where  $\mathbf{x}^* \in \mathbb{R}^N$  is sparse and  $\mathbf{A} \in \mathbb{R}^{M \times N}$  is a dictionary, sometimes referred to as the synthesis matrix, whose columns are the basis vectors.

This paper focuses on the SC problem of decomposing a signal into morphologically distinct components. A typical assumption for this problem is that the data is a linear combination of  $D$  source signals:

$$\mathbf{y} = \sum_{i=1}^D \mathbf{y}_i. \quad (2)$$

The MCA framework (Starck et al., 2004) requires that each component  $\mathbf{y}_i$  admits a sparse representation within the corresponding dictionary  $\mathbf{A}_i$ . The dictionaries  $\mathbf{A}_i$ s are distinct, i.e. each source-specific dictionary allows obtaining sparse representation of the corresponding source signal and is highly inefficient in representing the other content in the mixture. This leads to a signal model that generalizes the one given by Equation 1 as

$$\mathbf{y} \approx \sum_{i=1}^D \mathbf{A}_i \mathbf{x}_i^*. \quad (3)$$

The bottleneck of SC techniques is that at inference a sparse code has to be computed for each data point or data patch (as in case of high-resolution images) and this is typically done via iterative optimization. In case of single dictionary setting, ISTA (Daubechies et al., 2004) and FISTA (Beck & Teboulle, 2009) are classical algorithmic choices for this purpose. For the MCA problem, the standard choice is SALSA (Afonso et al., 2011), an instance of ADMM (Boyd et al., 2011). This process is prohibitively slow for high-throughput real-time applications.

The key contribution of this paper is an efficient and accurate deep learning architecture that is general enough to well-approximate optimal codes for both classic SC in a single-dictionary framework and MCA-based signal separation. We call our deep learning approximator Learned SALSA (LSALSA). The proposed encoder is formulated as a time-unfolded version of the SALSA algorithm with a fixed number of iterations, where the

depth of the deep learning model corresponds to the number of SALSA iterations. We train the deep model in the supervised fashion to predict optimal sparse codes for a given input and thus in practice we can use shallow architectures of fixed-depth that correspond to only few iterations of the original SALSA and achieve superior performance to this algorithm. Furthermore, SALSA comes with a built-in source separation mechanism and cross-iteration memory sharing connections. These main algorithmic features of SALSA translate to a specific connectivity pattern of the corresponding deep learning architecture of LSALSA that in consequence gives LSALSA an advantage over previous deep encoders, like LISTA (Gregor & LeCun, 2010), in terms of applicability to a broader class of learning problems (LISTA is used only in the single dictionary setting) and performance. To the best of our knowledge, our approach is the first one to utilize an instance of ADMM unrolled into a deep learning architecture to address a source separation problem.

This paper is organized as follows: Section 2 provides literature review, Section 3 formulates the SC problem in detail, Section 4 shows how to derive predictive single dictionary SC and multiple dictionary MCA from their iterative counterparts and explains our approach (LSALSA). Finally, Section 5 shows experimental results for both the single dictionary setting and MCA. Section 6 concludes the paper.

## 2. Related Work

A sparse code inference aims at computing sparse codes for given data and is most widely addressed via iterative schemes such as aforementioned ISTA and FISTA. Predicting approximations of optimal codes can be done using deep feed-forward learning architectures based on truncated convex solvers. This family of approaches lies at the core of this paper. A notable approach in this family known as LISTA (Gregor & LeCun, 2010) stems from earlier predictive sparse decomposition methods (Kavukcuoglu et al., 2010; Jarrett et al., 2009), which however were obtaining approximations to the sparse codes of insufficient quality. LISTA improves over these techniques and enhances ISTA by unfolding a fixed number of iterations to define a fixed-depth deep neural network that is trained with examples of input vectors paired with their corresponding optimal sparse codes obtained by conventional methods like ISTA or FISTA. LISTA was shown to provide high-quality approximations of optimal sparse codes with a fixed computational cost. Unrolling methodology has also been applied to algorithms solving SC with  $\ell_0$ -regularization (Wang et al., 2016) and message passing schemes (Borgerding & Schniter, 2016). In other prior works, ISTA was recast as a recurrent neural network unit giving rise to a variant of LSTM (Gers et al., 2003; Zhou et al., 2018). The above mentioned

algorithms do not suit well to the MCA problem as they have no algorithmic mechanism for handling multiple dictionaries. In other words, they would approach the MCA problem by casting it as a SC problem with access to a single dictionary that is a concatenation of source-specific dictionaries, e.g.  $[\mathbf{A}_1, \mathbf{A}_2, \dots, \mathbf{A}_D]$ .

This paper considers a generalization of the single-dictionary SC problem to the MCA framework. The framework assumes that the data can be explained by multiple distinct dictionaries. MCA has been used successfully in a number of applications that include decomposing images into textures and cartoons for denoising and inpainting (Starck et al., 2005b;a; Elad et al., 2005; Peyré et al., 2007; Shoham & Elad, 2008; Peyré et al., 2010), detecting text in natural scene images (Liu et al., 2017), as well as other source separation problems such as separating non-stationary clutter from weather radar signals (Uysal et al., 2016), transients from sustained rhythmic components in EEG signals (Parekh et al., 2014), and stationary from dynamic components of MRI videos (Otazo et al., 2015). The MCA problem is traditionally solved via SALSA algorithm, which constitutes a special case of the ADMM method.

There exist a few approaches in the literature utilizing ADMM unrolled into a deep learning architecture. One such computationally efficient framework (Sprechmann et al., 2013) was applied to learning task-specific (reconstruction or classification) sparse models via sparsity-promoting convolutional operators. Another unrolled version of ADMM (Yang et al., 2016) was demonstrated to improve the reconstruction accuracy and computational speed of baseline ADMM algorithm for the problem of compressive sensing Magnetic Resonance Imaging. A variety of papers followed up on this work for various image reconstruction tasks, such as the Learned Primal-dual Algorithm (Adler & Öktem, 2017). None of these approaches were applied to the MCA or other source separation problems. An unrolled nonnegative matrix factorization (NMF) algorithm (Le Roux et al., 2015) was implemented as a deep network for the task of speech separation. In another work (Wisdom et al., 2017), the NMF-based speech separation task was solved with an ISTA-like unfolded network.

## 3. Problem Formulation

This paper focuses on the inference problem in SC. It is formulated as finding the optimal sparse code  $\mathbf{x}^*$  given input vector  $\mathbf{y}$  and dictionary matrix  $\mathbf{A}$ , whose columns are the normalized basis vectors.  $\mathbf{x}^*$  minimizes the  $\ell_1$ -regularized linear least squares cost function

$$E_{\mathbf{A}}(\mathbf{x}; \mathbf{y}) = \frac{1}{2} \|\mathbf{y} - \mathbf{A} \mathbf{x}\|_2^2 + \alpha \|\mathbf{x}\|_1, \quad (4)$$

where the scalar constant  $\alpha \geq 0$  balances sparsity with data fidelity. Thus  $\mathbf{x}^* = \operatorname{argmin}_{\mathbf{x}} E_{\mathbf{A}}(\mathbf{x}; \mathbf{y})$  is the optimal code for  $\mathbf{y}$  with respect to  $\mathbf{A}$ . The dictionary

matrix  $\mathbf{A}$  is usually learned by minimizing a loss function given below (Olshausen & Field, 1996)

$$\mathcal{L}_{\text{Dict}}(\mathbf{A}) = \frac{1}{P} \sum_{p=1}^P E_{\mathbf{A}}(\mathbf{x}^{*,p}; \mathbf{y}^p) \quad (5)$$

with respect to  $\mathbf{A}$  using stochastic gradient descent (SGD), where  $P$  is the size of the training data set,  $\mathbf{y}^p$  is the  $p^{\text{th}}$  training sample, and  $\mathbf{x}^{*,p}$  is the corresponding optimal sparse code. The optimal sparse codes in each iteration are obtained in this paper with FISTA.

In the MCA framework, a generalization of the cost function from Equation 4 is minimized to estimate  $\mathbf{x}_1^*, \mathbf{x}_2^*, \dots, \mathbf{x}_D^*$  from the model given in Equation 3. Thus one minimizes

$$E_{\mathbf{A}}(\mathbf{x}; \mathbf{y}) = \frac{1}{2} \|\mathbf{y} - \mathbf{A} \mathbf{x}\|_2^2 + \sum_{i=1}^d \alpha_i \|\mathbf{x}_i\|_1, \quad (6)$$

where

$$\mathbf{A} := [\mathbf{A}_1, \mathbf{A}_2, \dots, \mathbf{A}_D] \in \mathbb{R}^{M \times N} \quad (7)$$

$$\mathbf{x} := [\mathbf{x}_1, \mathbf{x}_2, \dots, \mathbf{x}_D]^T \in \mathbb{R}^N, \quad (8)$$

where  $\mathbf{x}_i \in \mathbb{R}^{N_i}$  for  $i = \{1, 2, \dots, D\}$ ,  $N = \sum_{i=1}^D N_i$ , and  $\alpha_i$ s are the coefficients controlling the sparsity penalties. We denote the concatenated optimal codes with  $\mathbf{x}^* = \text{argmin}_{\mathbf{x}} E_{\mathbf{A}}(\mathbf{x}, \mathbf{y})$ .

In the classic MCA works, the dictionaries  $\mathbf{A}_i$ s are selected to be well-known filter banks with explicitly designed sparsification properties. Such hand-designed transforms have good generalization abilities and help to prevent overfitting. Also, MCA algorithms often require solving large systems of equations involving  $\mathbf{A}^T \mathbf{A}$  or  $\mathbf{A} \mathbf{A}^T$ . An appropriate constraining of  $\mathbf{A}_i$  leads to a banded system of equations and in consequence reduces the computational complexity of these algorithms, e.g.: (Parekh et al., 2014). More recent MCA works use learned dictionaries for image analysis (Shoham & Elad, 2008; Peyré et al., 2007). Some extensions of MCA consider learning dictionaries  $\mathbf{A}_i$ s and sparse codes jointly (Peyré et al., 2007; 2010). In our paper, we learn dictionaries  $\mathbf{A}_i$ s independently. In particular, for each  $i$  we minimize

$$\mathcal{L}_{\text{Dict}}(\mathbf{A}_i) = \frac{1}{P} \sum_{p=1}^P E_{\mathbf{A}_i}(\mathbf{x}_i^{*,p}; \mathbf{y}_i^p) \quad (9)$$

with respect to  $\mathbf{A}_i$  using SGD, where  $\mathbf{y}_i^p$  is the  $i^{\text{th}}$  mixture component of the  $p^{\text{th}}$  training sample and  $\mathbf{x}_i^{*,p}$  is the corresponding optimal sparse code. The optimal sparse codes in each iteration are obtained with FISTA.

## 4. From iterative to predictive SC and MCA

### 4.1. Split Augmented Lagrangian Shrinkage Algorithm (SALSA)

The objective functions used in SC (Equation 4) and MCA (Equation 6) are each convex with respect

---

### Algorithm 1 SALSA (Single Dictionary)

---

**Input:**  $\alpha \geq 0, \mu > 0, \mathbf{y} \in \mathbb{R}^M, \mathbf{A} \in \mathbb{R}^{M \times N}$

**Initialize:**  $\mathbf{x} = \mathbf{A}^T \mathbf{y}$  and  $\mathbf{d} = \mathbf{0}$

**repeat**

$\mathbf{u} = \text{soft}(\mathbf{x} + \mathbf{d}; \alpha/\mu)$

Solve for  $\mathbf{x}$ :  $[\mu \mathbf{I} + \mathbf{A}^T \mathbf{A}] \mathbf{x} = \mathbf{A}^T \mathbf{y} + \mu(\mathbf{u} - \mathbf{d})$

$\mathbf{d} = \mathbf{d} - \mathbf{u} + \mathbf{x}$

**until** change in  $\mathbf{x}$  below a threshold

---

to  $\mathbf{x}$ , allowing a wide variety of optimization algorithms with well-studied convergence results to be applied (Bauschke & Combettes, 2011). Here we describe a popular algorithm that is general enough to solve both problems called SALSA, which is an instance of ADMM.

ADMM addresses an optimization problem of the form

$$\min_{\mathbf{x}} f_1(\mathbf{x}) + f_2(\mathbf{x}) \quad (10)$$

by re-casting it as the equivalent, constrained problem

$$\min_{\mathbf{u}, \mathbf{x}} f_1(\mathbf{x}) + f_2(\mathbf{u}) \quad (11)$$

such that  $\mathbf{x} = \mathbf{u}$ .

ADMM then minimizes the corresponding augmented Lagrangian,

$$\mathcal{L}^A = f_1(\mathbf{x}) + f_2(\mathbf{u}) + \frac{\mu}{2} \|\mathbf{u} - \mathbf{x} - \mathbf{d}\|_2^2, \quad (12)$$

where  $\mathbf{d}$  correspond to Lagrangian multipliers, one variable at a time until convergence.

SALSA addresses an instance of the general optimization problem from Equation 11, where  $f_1$  is a least-squares term and  $f_2$  is such that its proximity operator can be computed exactly (Afonso et al., 2010). The algorithm falls under a sub-category of Douglas-Rachford Splitting methods, for which convergence has been proved (Eckstein & Bertsekas, 1992).

SALSA is given in Algorithms 1 and 2 for the single-dictionary case and the MCA case involving two dictionaries<sup>1</sup>, respectively, where

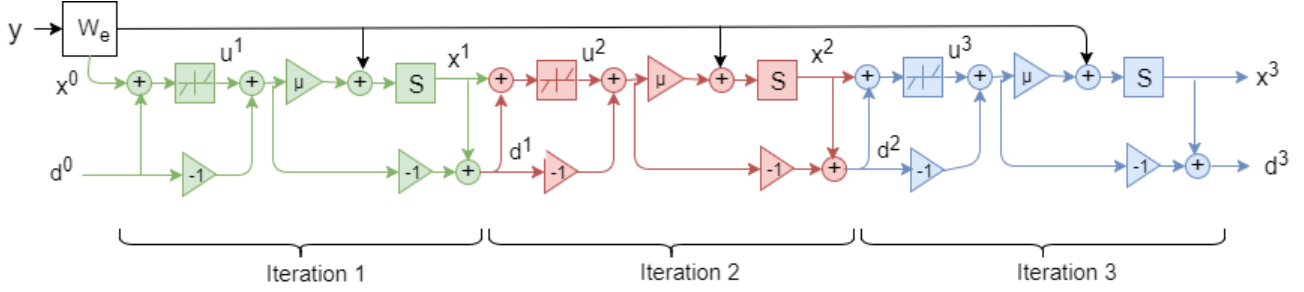
$$[\text{soft}(\mathbf{x}; \theta)]_i = \text{sign}(\mathbf{x}_i) (|\mathbf{x}_i| - \theta)_+ \quad (13)$$

is the soft-thresholding function with threshold  $\theta$ . Note that in Algorithm 2, the  $\mathbf{u}$  and  $\mathbf{d}$  updates can be performed with element-wise operations. The  $\mathbf{x}$ -update, however, is non-separable with respect to components for general  $\mathbf{A}$ . We call this the *splitting step*.

As mentioned in Section 3, the  $\mathbf{x}$ -update is often simplified to element-wise operations by constraining matrix

---

<sup>1</sup>In this paper we consider MCA framework with two dictionaries. Extensions to more than two dictionaries are straightforward.


 Figure 1: The deep learning architecture of LSALSA for  $T = 3$ .

**Algorithm 2** SALSA (Two Dictionaries)

**Input:**  $\alpha_1, \alpha_2 \geq 0, \mu > 0, \mathbf{y} \in \mathbb{R}^M, \mathbf{A} \in \mathbb{R}^{M \times (N_1 + N_2)}$

**Initialize:**  $\mathbf{x} = \mathbf{A}^T \mathbf{y}, \mathbf{d} := \begin{bmatrix} \mathbf{d}_1 \\ \mathbf{d}_2 \end{bmatrix} = 0;$

**repeat**

$$\mathbf{u} = \begin{bmatrix} \text{soft}(\mathbf{x}_1 + \mathbf{d}_1; \alpha_1/\mu) \\ \text{soft}(\mathbf{x}_2 + \mathbf{d}_2; \alpha_2/\mu) \end{bmatrix}$$

Solve for  $\mathbf{x}$ :  $[\mu \mathbf{I} + \mathbf{A}^T \mathbf{A}] \mathbf{x} = \mathbf{A}^T \mathbf{y} + \mu(\mathbf{u} - \mathbf{d})$

$\mathbf{d} = \mathbf{d} - \mathbf{u} + \mathbf{x}$

**until** change in  $\mathbf{x}$  below a threshold

**Algorithm 3** LSALSA (Single Dictionary): Forward Pass

**Input:**  $\alpha \geq 0, \mu > 0, \mathbf{y} \in \mathbb{R}^M$

$\mathbf{x}(0) = \mathbf{W}_e \mathbf{y}, \mathbf{d}(0) = 0$

**for**  $t = 1$  to  $T$  **do**

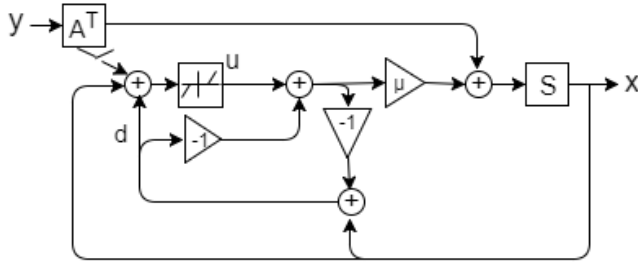
$\mathbf{u}(t) = \text{soft}(\mathbf{x}(t-1) + \mathbf{d}(t-1); \alpha/\mu)$

$\mathbf{x}(t) = \mathbf{S}(\mathbf{W}_e \mathbf{y} + \mu(\mathbf{u}(t) - \mathbf{d}(t-1)))$

$\mathbf{d}(t) = \mathbf{d}(t-1) - \mathbf{u}(t) + \mathbf{x}(t)$

**end for**

**Output:**  $\text{soft}(\mathbf{x}(t); \alpha/\mu)$


 Figure 2: A block diagram of SALSA. The one-time initialization  $\mathbf{x} = \mathbf{A}^T \mathbf{y}$  is represented by a gate on the left.

$\mathbf{A}$  to have special properties. For example: requiring  $\mathbf{A} \mathbf{A}^T = \rho \mathbf{I}$ ,  $\rho \in \mathbb{R}_+$ , reduces the  $\mathbf{x}$ -update step to element-wise division (after applying the matrix inverse lemma). In (Yang et al., 2016),  $\mathbf{A}$  is set to be the partial Fourier transform, reducing the system of equations of the  $\mathbf{x}$ -update to be a series of convolutions and element-wise operations. In our work, as is typical in the case of SC,  $\mathbf{A}$  is a learned dictionary without any imposed structure.

Note that solving for  $\mathbf{x}$  in Algorithms 1 and 2 requires the inversion of matrix  $\mu \mathbf{I} + \mathbf{A}^T \mathbf{A}$ . This however needs to be done just once, at the very beginning, as this matrix remains fixed during the entire run of SALSA. We abbreviate the inverted matrix as

$$\mathbf{S} = (\mu \mathbf{I} + \mathbf{A}^T \mathbf{A})^{-1}. \quad (14)$$

We call this matrix a *splitting operator*. The recursive block diagram of SALSA is depicted in Figure 2.

## 4.2. Learned SALSA (LSALSA)

We next describe our proposed deep encoder architecture that we refer to as Learned SALSA (LSALSA).

Consider truncating SALSA algorithm to a fixed number of iterations  $T$  and then time-unfolding it into a deep neural network architecture that matches the truncated SALSA's output exactly. The obtained architecture is illustrated in Figure 1 for  $T = 3$ .

We initialize the parameters of the deep model with

$$\mathbf{W}_e = \mathbf{A}^T \in \mathbb{R}^{N \times M} \quad (15)$$

$$\mathbf{S} = (\mu \mathbf{I} + \mathbf{A}^T \mathbf{A})^{-1} \in \mathbb{R}^{N \times N}, \quad (16)$$

where  $N = N_1 + N_2$  in the MCA case, to achieve an exact correspondence with SALSA. All splitting operators  $\mathbf{S}$  share parameters across the network.

LSALSA can be trained with a standard backpropagation. Let  $\mathbf{x} = f_e(\mathbf{W}_e, \mathbf{S}, \mathbf{y})$  denote the output of the LSALSA architecture. The cost function used for training the model is defined as

$$\mathcal{L}(\mathbf{W}_e, \mathbf{S}) = \frac{1}{2P} \sum_{p=1}^P \|\mathbf{x}^{*,p} - f_e(\mathbf{W}_e, \mathbf{S}, \mathbf{y}^p)\|_2^2. \quad (17)$$

The pseudocodes for computing a forward-pass through LSALSA are given in Algorithm 3 and Algorithm 4 for the single-dictionary and MCA cases, respectively.

## 4.3. LSALSA versus LISTA

Here we explain the conceptual difference between LSALSA and LISTA (see also Section A in the Supplement). This difference is a direct consequence of a

---

**Algorithm 4** LSALSA (Two Dictionaries): Forward Pass

---

**Input:**  $\alpha_1, \alpha_2 \geq 0, \mu > 0, \mathbf{y} \in \mathbb{R}^M$   
 $\mathbf{x}(0) = \mathbf{W}_e \mathbf{y}, \mathbf{d}(0) = 0$   
**for**  $t = 1$  **to**  $T$  **do**  
 $\mathbf{u}(t) = \begin{bmatrix} \text{soft}(\mathbf{x}_1(t-1) + \mathbf{d}_1(t-1); \alpha_1/\mu) \\ \text{soft}(\mathbf{x}_2(t-1) + \mathbf{d}_2(t-1); \alpha_2/\mu) \end{bmatrix}$   
 $\mathbf{x}(t) = \mathbf{S}(\mathbf{W}_e \mathbf{y} + \mu(\mathbf{u}(t) - \mathbf{d}(t-1)))$   
 $\mathbf{d}(t) = \mathbf{d}(t-1) - \mathbf{u}(t) + \mathbf{x}(t)$   
**end for**  
**Output:**  $\begin{bmatrix} \text{soft}(\mathbf{x}_1(t); \alpha_1/\mu) \\ \text{soft}(\mathbf{x}_2(t); \alpha_2/\mu) \end{bmatrix}$

---

different nature of their maternal algorithms, SALSA and ISTA respectively. ISTA is a proximal gradient method that solves the optimization problem of Equation 4 by iteratively repeating gradient descent step followed by soft thresholding. SALSA on the other hand is a second-order method that recasts the problem in terms of constrained optimization and optimizes the corresponding Augmented Lagrangian. Consequently, LISTA has a simple structure such that each layer depends only on the previous layer and re-injection of the filtered data  $\mathbf{W}_e \mathbf{y}$  (see (Gregor & LeCun, 2010) for reference). LSALSA has cross-layer connections resulting from the existence of the Lagrangian multiplier update (the  $\mathbf{d}$ -step) in the SALSA algorithm, which allows for learning dependencies between non-adjacent layers.

## 5. Experimental Results

We run different optimization algorithms to predict optimal codes for various data sets and for a varying number of iterations ( $T$ ). We provide empirical evaluation for both one and two-dictionary (MCA) settings. We focus on the inference problem and thus for each experiment the dictionaries were learned off-line and used for all methods (the visualization of the atoms of the obtained dictionaries can be found in Section B in the Supplement). We compare the following methods: LSALSA, truncated SALSA, truncated FISTA, and LISTA. Both LSALSA and LISTA are implemented as feedforward neural networks. For MCA experiments, we simply run FISTA and LISTA using the concatenated dictionary A.

### 5.1. Single Dictionary Case

We run experiments with four data sets: Fashion MNIST (Xiao et al., 2017) (10 classes), ASIRRA (Elson et al., 2007) (2 classes), MNIST (LeCun et al., 2009) (10 classes), and CIFAR-10 (Krizhevsky & Hinton, 2009) (10 classes). The ASIRRA data set is a collection of natural images of cats and dogs. We use a subset of the whole data set: 4000 training images and 1000 testing

images as commonly done (Golle, 2008). The results for MNIST and CIFAR-10 are reported in Section C in the Supplement.

The  $32 \times 32$  Fashion MNIST images were first divided into  $10 \times 10$  non-overlapping patches (ignoring extra pixels on two edges), resulting in 9 patches per image. Then, optimal codes were computed for each vectorized patch by minimizing the objective from Equation 4 with FISTA for 200 iterations. The ASIRRA images come in varying sizes. We resized them all to the resolution of  $224 \times 224$  and converted them to grayscale. Then we divided them into  $16 \times 16$  non-overlapping patches, resulting in 196 patches per image. Optimal codes were computed patch-wise as for Fashion MNIST, but taking 700 iterations to ensure convergence on this more difficult SC problem. For both data sets,  $\alpha$  was chosen so that the sparsity level was about 90%.

The data sets were then separated into training and testing sets. The training patches were used to produce the dictionaries. Visualizations of the dictionary atoms are provided in Section B in the Supplement. An exhaustive hyper-parameter search was performed for each encoding method and for each number of iterations  $T$ , to minimize RMSE between obtained and optimal codes. The hyper-parameters search included  $\alpha$  for all methods,  $\mu$  for SALSA and LSALSA, as well as learning rates and learning rate decays for LSALSA and LISTA.

The obtained encoders were used to compute sparse codes on the test set. Those were then compared with the optimal codes via RMSE. The results for Fashion MNIST are shown in terms of the number of iterations (Figure 3) and the wallclock time in seconds (Figure 4) used to make the prediction. It takes FISTA more than 15 iterations and SALSA more than 5 to reach the error achieved by LSALSA in just one. Near  $T = 100$ , both FISTA and SALSA are finally converging to the optimal codes. LISTA outperforms FISTA at first, but does not show much improvement after  $T > 10$ . Similar results for ASIRRA are shown in Figures 5 and 6. On this more difficult problem, it takes FISTA more than 50 iterations and SALSA more than 20 to catch up with LSALSA with a single iteration. LISTA and LSALSA are comparable for  $T \leq 5$ , after which LSALSA dramatically improves its optimal code prediction and, similarly as in case of Fashion MNIST, shows advantage in terms of the number of iterations, wallclock time, and the quality of the recovered sparse codes over other methods.

We also investigated which method yields better codes in terms of the classification task. For each data set, we trained a logistic regression classifier to predict the label from the corresponding sparse code. Thus, for Fashion MNIST each image is associated with 9 optimal codes (one for each patch), yielding a total feature length of  $9 \times 10 \times 10 = 900$ . The Fashion MNIST classifier was

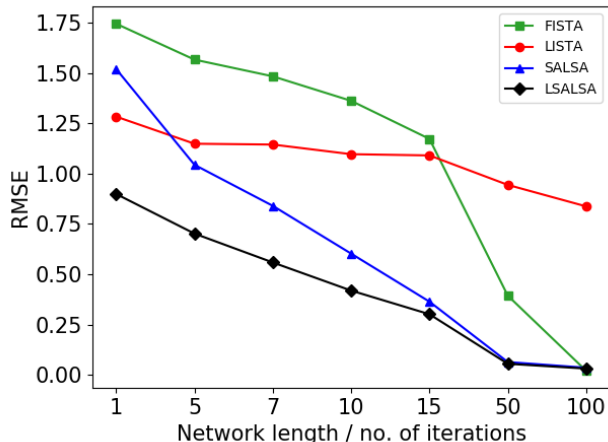


Figure 3: Fashion MNIST code prediction errors for varying numbers of iterations.

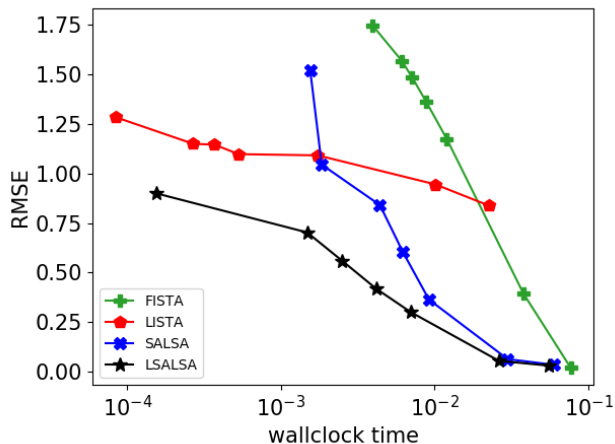


Figure 4: Fashion MNIST code prediction error as a function of the wallclock time.

trained until it achieved 0% classification error on the testing set. For ASIRRA, each concatenated optimal code had length  $196 \times 16 \times 16 = 50176$ ; to reduce the dimensionality we applied a random Gaussian projection  $\mathcal{G} : \mathbb{R}^{50176} \rightarrow \mathbb{R}^{500}$  before inputting the codes into the classifier. The classifier was trained on the optimal projected codes of length 500 until it achieved 0.5% error. The results for Fashion MNIST and ASIRRA are shown in Table 1 and 2, respectively. *Note:* The classifier was trained on the optimal codes for images from a test set. Thus, the resulting classification error is only due to the difference between the optimal and estimated codes.

## 5.2. MCA: Two-Dictionary Case

We first describe the data set that we use for the MCA experiments. Following the notation introduced previously in the paper, we set  $\mathbf{y}_1^p$ s to be the whole  $32 \times 32$  MNIST images and  $\mathbf{y}_2^p$ s to be the non-overlapping  $32 \times 32$  patches from ASIRRA (thus we have 49 patches per image). We obtain 196k training and 49k testing

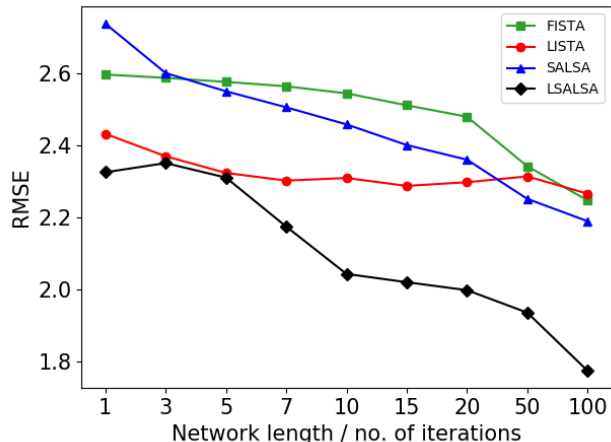


Figure 5: ASIRRA code prediction errors for varying numbers of iterations.

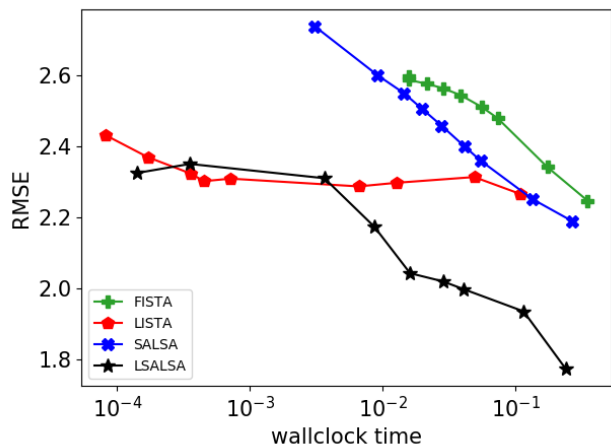


Figure 6: ASIRRA code prediction error as a function of the wallclock time.

Iter	Classification Error (in %)			
	FISTA	LISTA	SALSA	LSALSA
1	87.5312	54.6056	56.4777	<b>11.2252</b>
5	78.4570	38.1251	23.6107	<b>3.1798</b>
7	70.2489	37.1643	9.1991	<b>0.6628</b>
10	56.0629	32.9025	1.5871	<b>0.0755</b>
15	31.9948	30.4471	<b>0.0000</b>	<b>0.0000</b>
50	0.1011	14.0294	<b>0.0000</b>	<b>0.0000</b>
100	<b>0.0000</b>	7.9534	<b>0.0000</b>	<b>0.0000</b>

Table 1: Fashion-MNIST classification results. The best performer is in bold. All methods but LISTA were able to match the optimal codes well enough to get zero percent error by  $T = 100$ .

patches from ASIRRA, and 60k training and 10k testing images from MNIST. We randomly mix images from MNIST and patches from ASIRRA and generate 588k mixed training images and 49k mixed testing images. Optimal codes were computed using SALSA (Algorithm 2) for 100 iterations, ensuring that both components had a sparsity level around 90%. Note

Iter	Classification Error (in %)			
	FISTA	LISTA	SALSA	LSALSA
1	48.9000	52.4000	48.8000	<b>40.1000</b>
3	49.2000	52.7000	46.0000	<b>42.8000</b>
5	48.5000	53.5000	44.8000	<b>35.0000</b>
7	47.8000	53.7000	44.5000	<b>35.1000</b>
10	46.5000	38.5000	42.7000	<b>34.4000</b>
15	43.9000	38.1000	40.7000	<b>33.1000</b>
20	42.1000	37.6000	38.7000	<b>31.6000</b>
50	37.8000	38.2000	37.2000	<b>31.9000</b>
100	36.4000	37.1000	36.8000	<b>30.8000</b>

Table 2: ASIRRA classification results. The best performer is in bold.

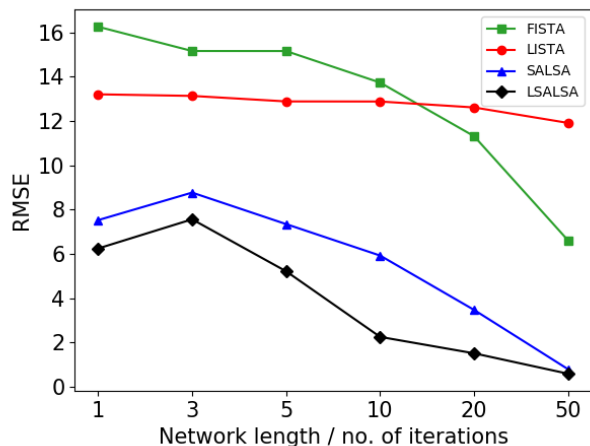


Figure 8: MCA experiment using MNIST + ASIRRA data set. Code prediction errors for varying numbers of iterations. LISTA saturates very fast as it does not support unmixing signals.

that we also performed experiments on a mixed dataset of CIFAR-10 and MNIST. Those can be found in Section D in the Supplement.

An exhaustive hyper-parameter search was performed for each encoding method and for each number of iterations  $T$ . The hyper-parameters search included  $\alpha$  for FISTA and LISTA,  $\alpha_1, \alpha_2, \mu$  for SALSA and

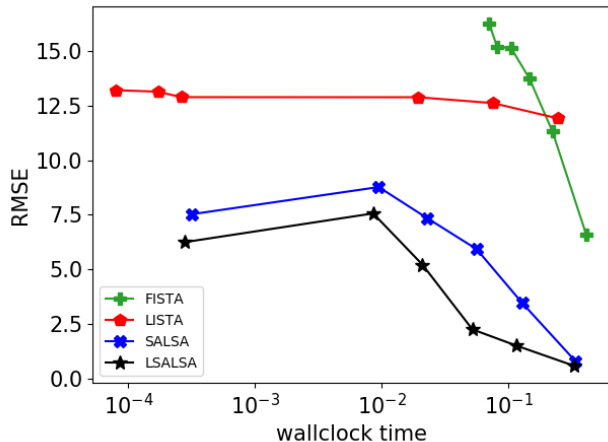


Figure 9: MCA experiment using MNIST + ASIRRA data set. Code prediction error versus wallclock time.

LSALSA, as well as learning rates for LSALSA and LISTA.

Code prediction error curves are presented in Figure 8 and 9. LSALSA steadily outperforms the others, until SALSA catches up around  $T = 50$ . FISTA and LISTA, without a mechanism for distinguishing two dictionaries, struggle to estimate the optimal codes.

In Figure 7 we illustrate each method’s sparsity/accuracy trade-off on the ASIRRA test data set, while varying  $T$  (Section E in the Supplement shows the same plot for a wider variety of  $T$  as well as contains a similar plot for MNIST). The LSALSA retains both the highest sparsity and accuracy levels, even for small  $T$ , from among all the methods.

Similarly as before, we performed an evaluation on the classification task. A separate classifier was trained for each data set using the separated optimal codes  $\mathbf{x}_1^{*,p}$  and  $\mathbf{x}_2^{*,p}$ , respectively. As before, a random Gaussian projection was used to reduce the ASIRRA codes to the length 500 before inputting to the classifier. The classification results are depicted in Table 3 for MNIST and Table 4 for ASIRRA.

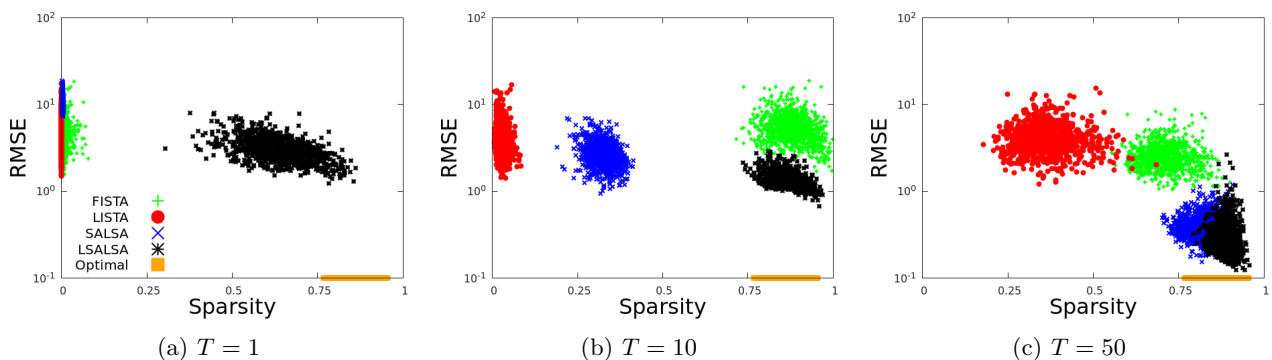


Figure 7: Sparsity/accuracy trade-off analysis for ASIRRA obtained for the source separation experiment with MNIST + ASIRRA data set. Each method corresponds to a colored point cloud, where each point corresponds to one sample from the ASIRRA test data set. LSALSA achieves the best sparsity/accuracy trade-off and is faster than other methods.

Iter	Classification Error (in %)			
	FISTA	LISTA	SALSA	LSALSA
1	70.2886	16.8114	26.9935	<b>2.3720</b>
3	34.0881	16.0946	24.4524	<b>3.6885</b>
5	89.9683	14.7785	39.7438	<b>1.1499</b>
10	90.0000	15.0006	3.0251	<b>0.0520</b>
20	90.0000	9.7423	0.8543	<b>0.0495</b>
50	1.2976	6.7252	0.0243	<b>0.0184</b>

Table 3: MNIST classification error obtained after source separation. The best performer is in bold.

Iter	Classification Error (in %)			
	FISTA	LISTA	SALSA	LSALSA
1	43.7000	39.8000	46.7000	<b>32.6000</b>
3	41.5000	40.2000	42.4000	<b>35.3000</b>
5	49.8000	38.8000	43.8000	<b>30.0000</b>
10	49.9000	38.6000	28.9000	<b>22.3000</b>
20	45.5000	37.9000	23.0000	<b>19.1000</b>
50	28.4000	36.4000	<b>12.4000</b>	12.7000

Table 4: ASIRRA classification error obtained after source separation. The best performer is in bold.

Finally, in Figure 10 we present exemplary reconstructed images obtained by different methods when performing source separation (more reconstruction results can be found in Section F in the Supplement). No additional learning was performed to achieve reconstruction, the estimated codes were simply multiplied by the corresponding dictionary matrix, i.e. for LSALSA we have  $\mathbf{A}_i \cdot (f_e(\mathbf{W}_e, \mathbf{S}, \mathbf{y}))_i$ , where  $f_e(\mathbf{W}_e, \mathbf{S}, \mathbf{y})_i$  represents the  $i$ -th component of an encoder’s output. FISTA and LISTA are unable to separate components without severely corrupting the ASIRRA component. LSALSA has visually recognizable separations even at  $T = 1$ , and the MNIST component is almost gone by  $T = 5$ .

## 6. Conclusions

In this paper we propose a deep encoder architecture LSALSA obtained from time-unfolding the Split Augmented Lagrangian Shrinkage Algorithm (SALSA). We demonstrate that LSALSA outperforms baseline methods such as SALSA, FISTA, and LISTA, in terms of the quality of predicted sparse codes, as well as the running time in both the single and multiple (MCA) dictionary case. In the two-dictionary MCA setting, we furthermore show that LSALSA obtains the separation of image components that has better visual quality than the separation obtained by SALSA.

## References

- Adler, J. and Öktem, O. Learned primal-dual reconstruction. *CoRR*, abs/1707.06474, 2017.
- Afonso, M., Biucas-Dias, J., and Figueiredo, M. Fast

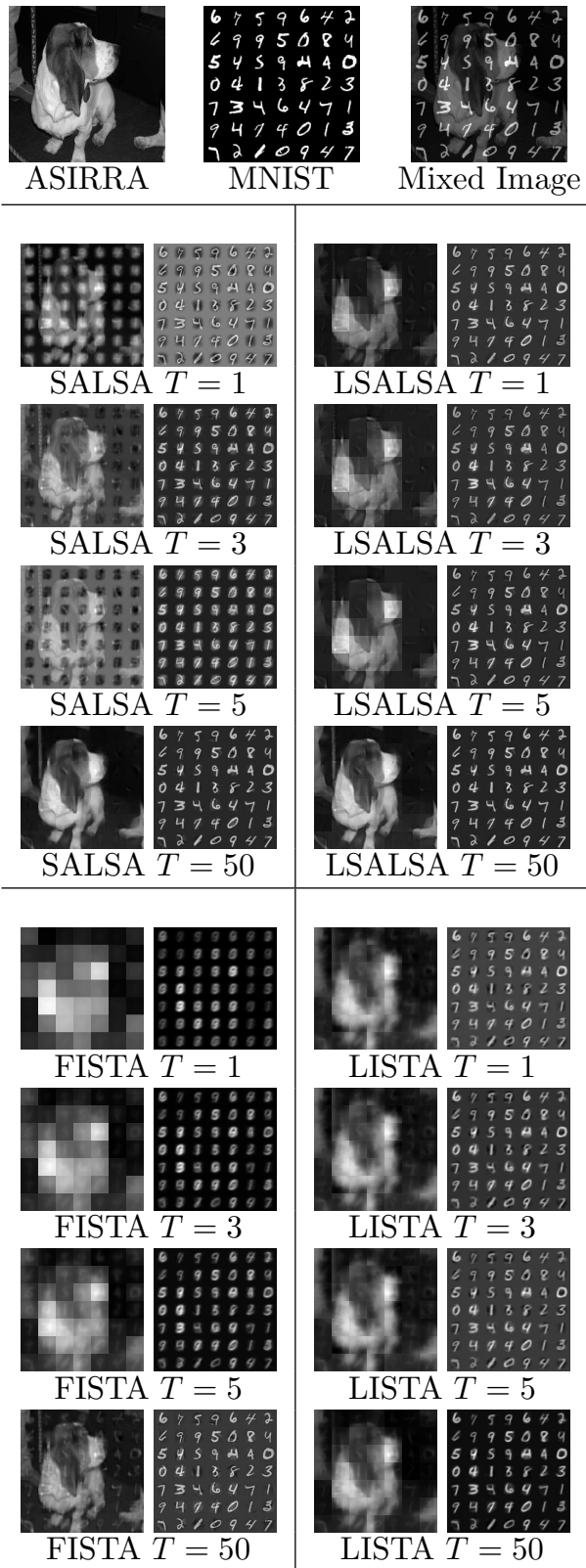


Figure 10: MCA experiment. Image reconstructions obtained by SALSA, LSALSA, FISTA, LISTA for  $T = 1, 3, 5, 50$ . Top row: original data (components and mixed).

- image recovery using variable splitting and constrained optimization. *IEEE Trans. Image Processing*, 19(9):2345–2356, 2010.
- Afonso, M., Bioucas-Dias, J., and Figueiredo, M. An augmented lagrangian approach to the constrained optimization formulation of imaging inverse problems. *Trans. Img. Proc.*, 20(3):681–695, 2011.
- Bauschke, H. H. and Combettes, P. L. *Convex Analysis and Monotone Operator Theory in Hilbert Spaces*. Springer Publishing Company, 1st edition, 2011.
- Beck, A. and Teboulle, M. A fast iterative shrinkage-thresholding algorithm for linear inverse problems. *SIAM J. Img. Sci.*, 2(1):183–202, 2009.
- Borgerding, M. and Schniter, P. Onsager-corrected deep learning for sparse linear inverse problems. In *GlobalSIP*, 2016.
- Boyd, S., Parikh, N., Chu, E., Peleato, B., and Eckstein, J. Distributed optimization and statistical learning via the alternating direction method of multipliers. *Foundations and Trends in Machine Learning*, 3(1): 1–122, 2011.
- Daubechies, I., Defrise, M., and De Mol, C. An iterative thresholding algorithm for linear inverse problems with a sparsity constraint. *Communications on Pure and Applied Mathematics*, 57(11):1413–1457, 2004.
- Eckstein, J. and Bertsekas, D. On the douglas-rachford splitting method and the proximal point algorithm for maximal monotone operators. *Math. Program.*, 55:293–318, 1992.
- Elad, M., Starck, J. L., Querre, P., and Donoho, D. L. Simultaneous cartoon and texture image inpainting using morphological component analysis (mca). *Applied and Computational Harmonic Analysis*, 19(3): 340–358, 2005.
- Elson, J., Douceur, J., Howell, J., and Saul, J. Asirra: a captcha that exploits interest-aligned manual image categorization. In *ACM CCS*, 2007.
- Gers, F. A., Schraudolph, N. N., and Schmidhuber, J. Learning precise timing with lstm recurrent networks. *J. Mach. Learn. Res.*, 3:115–143, 2003.
- Golle, P. Machine learning attacks against the asirra captcha. In *ACM CCS*, 2008.
- Gregor, K. and LeCun, Y. Learning fast approximations of sparse coding. In *ICML*, 2010.
- Jarrett, K., Kavukcuoglu, K., Koray, M., and LeCun, Y. What is the best multi-stage architecture for object recognition? In *ICCV*, 2009.
- Kavukcuoglu, K., Ranzato, M. A., and LeCun, Y. Fast inference in sparse coding algorithms with applications to object recognition. *CoRR*, abs/1010.3467, 2010.
- Krizhevsky, A. and Hinton, G. Learning multiple layers of features from tiny images, 2009.
- Le Roux, J., Hershey, J. R., and Wenginger, F. Deep nmf for speech separation. In *ICASSP*, 2015.
- LeCun, Y., Bottou, L., Bengio, Y., and Haffner, P. Gradient-based learning applied to document recognition. In *Proceedings of the IEEE*, 2009.
- Liu, S., Xian, Y., Li, H., and Yu, Z. Text detection in natural scene images using morphological component analysis and laplacian dictionary. *IEEE/CAA Journal of Automatica Sinica*, PP(99):1–9, 2017.
- Olshausen, B. and Field, D. Emergence of simple-cell receptive field properties by learning a sparse code for natural images. *Nature*, 381:607–609, 1996.
- Otazo, R., Candès, E., and Sodickson, D. K. Low-rank and sparse matrix decomposition for accelerated dynamic mri with separation of background and dynamic components. *Magn Reson Med*, 73(3):1125–36, 2015.
- Parekh, A., Selesnick, I., Rapoport, D., and Ayappa, I. Sleep spindle detection using time-frequency sparsity. In *IEEE SPMB*, 2014.
- Peyré, G., J.Fadili, and Starck, J.-L. Learning adapted dictionaries for geometry and texture separation. In *SPIE Wavelets*, 2007.
- Peyré, G., J.Fadili, and Starck, J.-L. Learning the morphological diversity. *SIAM J. Imaging Sciences*, 3(3):646–669, 2010.
- Shoham, N. and Elad, M. Algorithms for signal separation exploiting sparse representations, with application to texture image separation. In *Proceedings of the IEEE 25th Convention of Electrical and Electronics Engineers in Israel*, 2008.
- Sprechmann, P., Litman, R., Yakar, T., Bronstein, A., and Sapiro, G. Efficient supervised sparse analysis and synthesis operators. In *NIPS*, 2013.
- Starck, J.-L., Elad, M., and Donoho, D. Redundant multiscale transforms and their application for morphological component separation. *Advances in Imaging and Electron Physics - ADV IMAG ELECTRON PHYS*, 132:287–348, 2004.
- Starck, J.-L., Elad, M., and Donoho, D. Image decomposition via the combination of sparse representations and a variational approach. *IEEE Trans. Image Processing*, 14(10):1570–1582, 2005a.

- Starck, J.-L., Moudden, Y., J.Bobina, Elad, M., and Donoho, D. Morphological component analysis. In *Proc. SPIE Wavelets*, 2005b.
- Uysal, F., Selesnick, I., and Isom, B. Mitigation of wind turbine clutter for weather radar by signal separation. *IEEE Trans. Geoscience and Remote Sensing*, 54(5): 2925–2934, 2016.
- Wang, Z., Ling, Q., and Huang, T. Learning deep 10 encoders. In *AAAI*, 2016.
- Wisdom, S., Powers, T., Pitton, J., and Atlas, L. Deep recurrent nmf for speech separation by unfolding iterative thresholding. *IEEE Workshop on Applications of Signal Processing to Audio and Acoustics (WASPAA)*, pp. 254–258, 2017.
- Xiao, H., Rasul, K., and Vollgraf, R. Fashion-mnist: a novel image dataset for benchmarking machine learning algorithms. *CoRR*, abs/1708.07747, 2017.
- Yang, Y., Sun, J., Li, H., and Xu, Z. Deep admm-net for compressive sensing mri. In *NIPS*, 2016.
- Zhou, J., Di, K., Du, J., Peng, X., Yang, H., S. Pan, I. Tsang, Liu, Y., Qin, Z., and Goh, R. Sc2net: Sparse lstms for sparse coding. In *AAAI*, 2018.

---

# LSALSA: efficient sparse coding in single and multiple dictionary settings

## (Supplementary material)

---

### A. Additional discussion on the difference between LSALSA and LISTA

The recursive formula in LISTA is given as

$$\mathbf{u}(t+1) = \text{soft}(\mathbf{A}^T \mathbf{y} + \mathbf{S} \mathbf{u}(t)). \quad (18)$$

The recursive formula in LSALSA is derived below. We start with the output of the  $(t+1)^{\text{th}}$  non-linearity from Algorithm 1:

$$\mathbf{u}(t+1) = \text{soft}(\mathbf{x}(t) + \mathbf{d}(t)) \quad (19)$$

$$\mathbf{u}(t+1) = \text{soft}(\underbrace{\mathbf{S}(\mathbf{W}_e \mathbf{y} + \mu(\mathbf{u}(t) - \mathbf{d}(t-1)))}_{\mathbf{x}(t)} + \underbrace{\mathbf{d}(t-1) - \mathbf{u}(t) + \mathbf{x}(t)}_{\mathbf{d}(t)}) \quad (20)$$

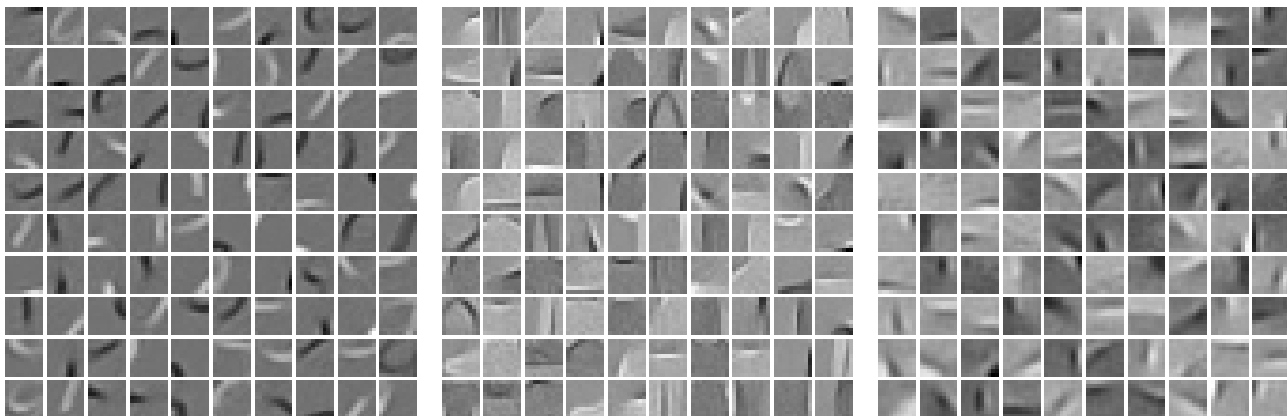
$$\mathbf{u}(t+1) = \text{soft} \left\{ \left[ \left( \sum_{k=1}^t M^{t-k} + M^{t-1} \right) \mathbf{S} + \mathbf{I} \right] \mathbf{A}^T \mathbf{y} + \sum_{k=1}^t \left[ (\mu M^{t-k} \mathbf{S} - \mathbf{I}) \mathbf{u}(k) + \mu \sum_{i=1}^k M^{k-i} \mathbf{S} \mathbf{u}(i) \right] \right\}, \quad (21)$$

where  $M = I - \mu \mathbf{S}$ , and  $\mathbf{u}(t)$  is the output of the  $t^{\text{th}}$  network non-linearity. Clearly, in the case of LSALSA, the non-linearity output  $\mathbf{u}(t+1)$  has a dependence on *all* of the previous layers' outputs. This comes from the auxiliary variable  $\mathbf{d}$ , i.e. the Lagrangian multipliers term. LISTA's  $t^{\text{th}}$  output only depends directly on the previous layer.

### B. Dictionary Learning Experiments

We visualize the learned dictionary atoms for both single (Figure 11 and 12) and two dictionary (MCA) case (Figure 13, and 14).

#### B.1. Dictionaries used in single dictionary experiments



(a)

(b)

(c)

Figure 11: Visualization of dictionary atoms trained on (a)  $10 \times 10$  MNIST image patches (b)  $10 \times 10$  Fashion-MNIST image patches (c)  $10 \times 10$  CIFAR-10 image patches. Each dictionary has 100 atoms (complete) and each atom is a unit norm vector of length 100 reshaped to  $10 \times 10$ .

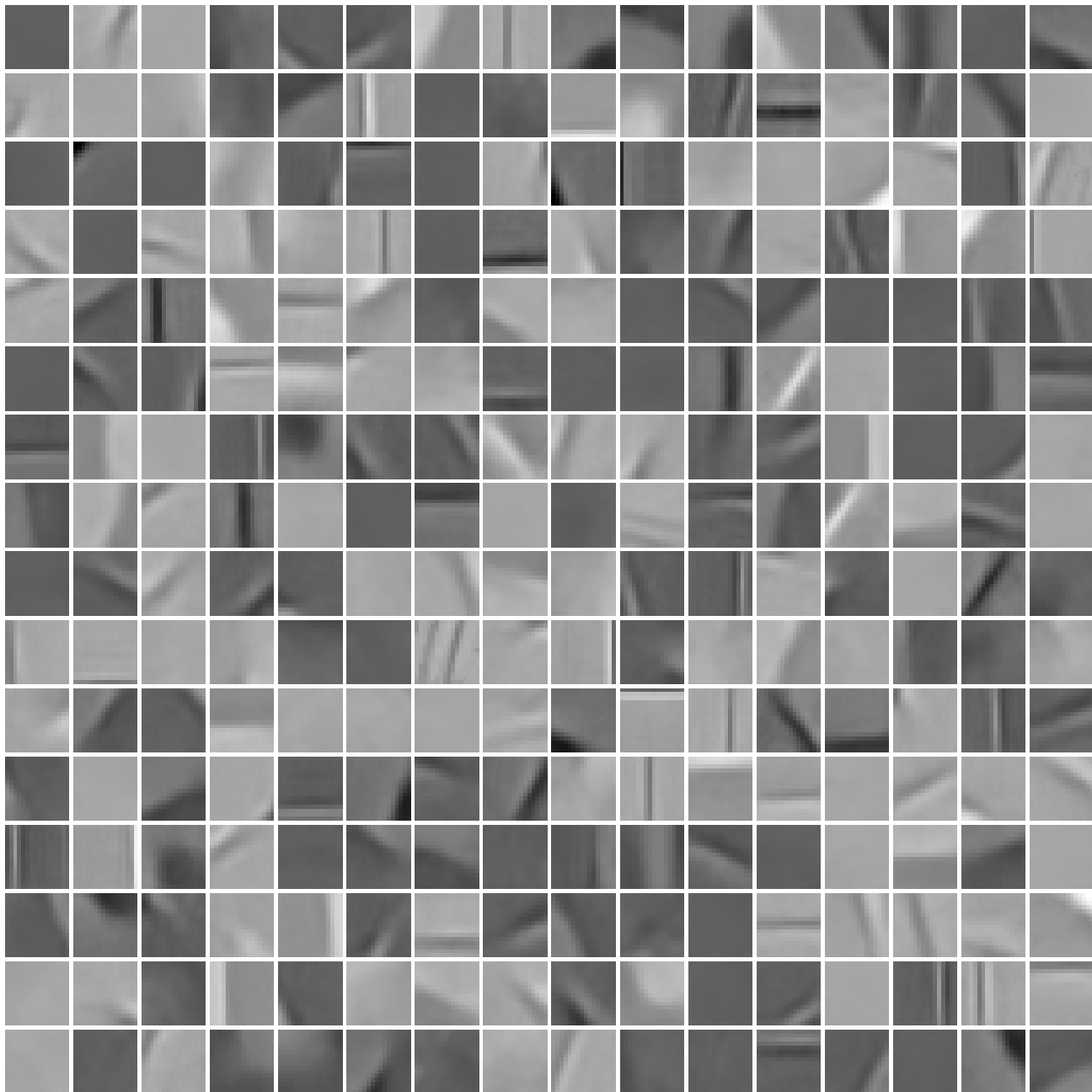


Figure 12: Visualization of ASIRRA dictionary trained on  $16 \times 16$  image patches. The dictionary has 256 (complete) atoms and each atom is a unit norm vector of length 256 reshaped to  $16 \times 16$ .

## B.2. Dictionaries used in MCA experiments

In the first set of MCA experiments we performed source separation on  $32 \times 32$  MNIST + ASIRRA images. We used two dictionaries trained independently using whole  $32 \times 32$  MNIST images and  $32 \times 32$  patches of ASIRRA images. In the second set of MCA experiments, we performed source separation on spatially added MNIST and CIFAR-10 images (more results of this experiment showed in Section D of the Supplement). We used same MNIST dictionary as used in MNIST + ASSIRA experiments and trained a CIFAR-10 dictionary on the whole  $32 \times 32$  grayscale CIFAR-10 data set images. These dictionaries have 1024 atoms (complete), all normalized vectors of length 1024 reshaped to  $32 \times 32$ . A subset of atoms of the dictionaries used in MCA experiments are visualized in Figure 13 and Figure 14.

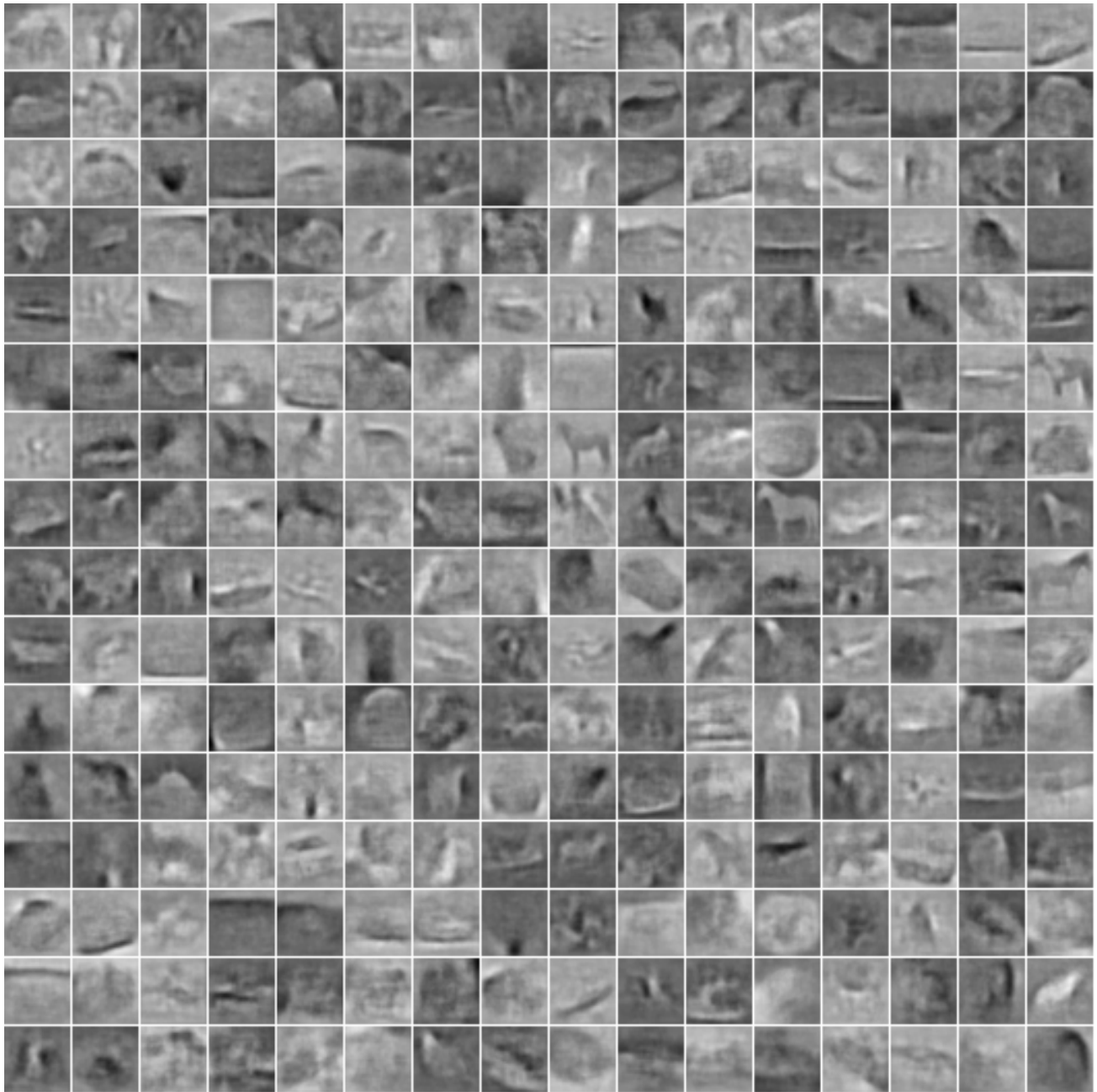
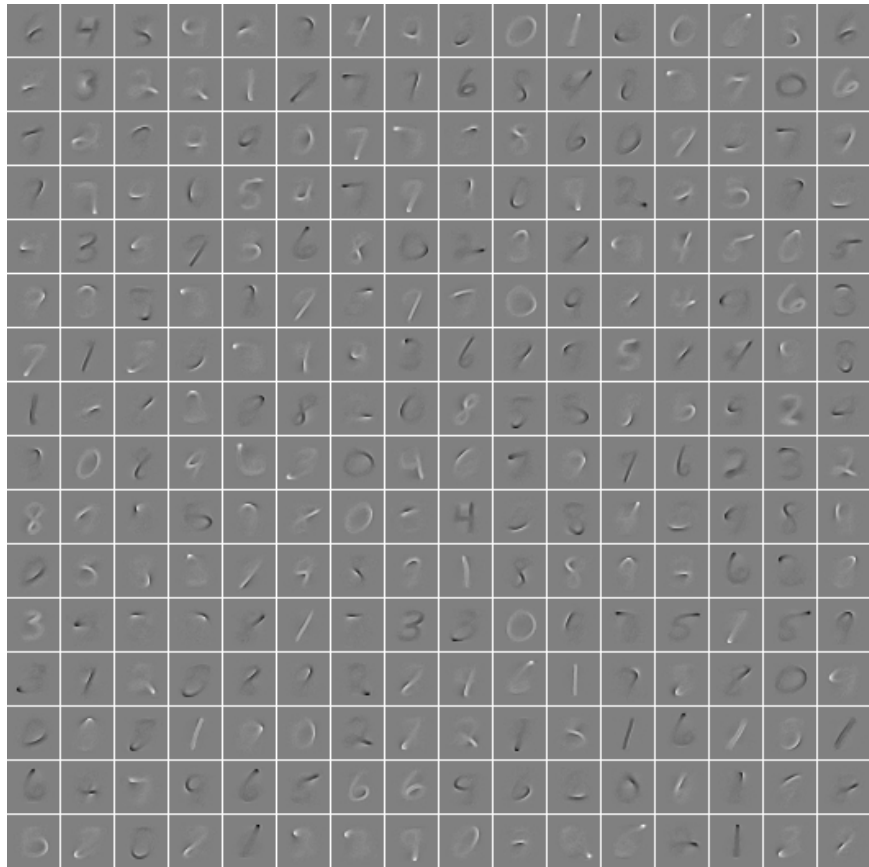
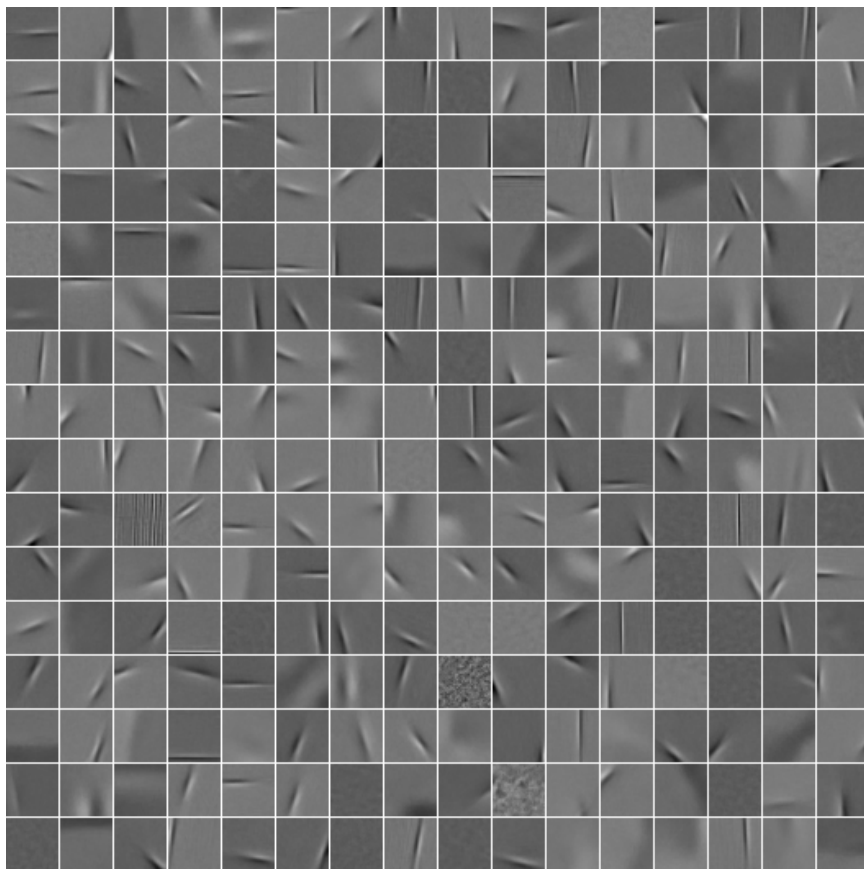


Figure 13: Visualization of dictionary atoms trained on  $32 \times 32$  CIFAR-10 images.



(a)



(b)

Figure 14: Visualization of dictionary atoms trained on (a)  $32 \times 32$  MNIST images and (b)  $32 \times 32$  ASIRRA image patches.

## C. Additional single dictionary experiments

The single dictionary experiments on MNIST and CIFAR-10 data sets are summarized below. The code prediction errors for MNIST are captured in Figure 15 and for CIFAR are captured in Figure 16. The classification results are captured in Table 5 for MNIST and Table 6 for CIFAR.

### C.1. MNIST

The  $32 \times 32$  MNIST images were first scaled to pixel values in range  $[0, 1]$  and then divided into  $10 \times 10$  non-overlapping patches (ignoring extra pixels on edges), resulting in 9 patches per image. Only patches with standard deviation  $\geq 0.1$  were used in training and the remaining ones were discarded (as they are practically all-black). Optimal codes were computed for each vectorized patch by minimizing the objective from Equation 4 by running FISTA for 200 iterations giving approximately 95% sparse optimal codes.

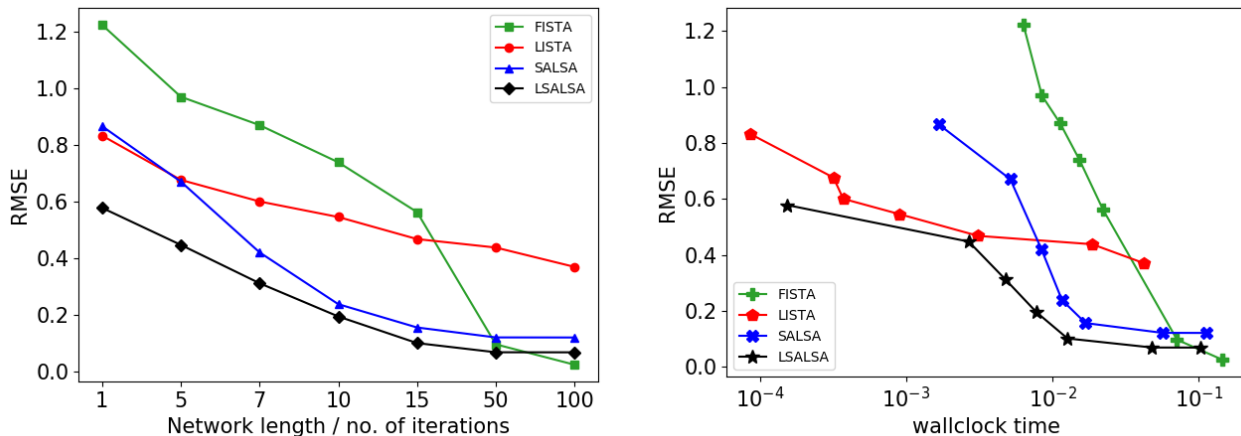


Figure 15: (Left:) MNIST code prediction errors for varying numbers of iterations. FISTA takes 15 iterations to give error produced by 1 iteration of LSALSA. FISTA estimates optimal codes better than LISTA for higher  $T$ . (Right:) MNIST code prediction error as a function of the wallclock time.

Iter	Classification Error (in %)			
	FISTA	LISTA	SALSAs	LSALSA
1	40.8682	4.5842	20.7291	<b>1.9130</b>
5	6.1046	4.6527	4.8549	<b>1.7773</b>
7	3.4363	2.0406	0.8097	<b>0.4574</b>
10	2.0326	1.3802	<b>0.0990</b>	0.0996
15	1.0725	0.8778	0.0200	<b>0.0103</b>
50	0.0205	0.6168	<b>0.0000</b>	<b>0.0000</b>
100	<b>0.0000</b>	0.4228	<b>0.0000</b>	<b>0.0000</b>

Table 5: MNIST classification results. The best performer is in bold.

### C.2. CIFAR-10

In CIFAR-10 experiments,  $32 \times 32$  natural images were first converted to grayscale, scaled to values in range  $[0, 1]$ , and broken down to  $10 \times 10$  non-overlapping patches. Each image resulted in 9 patches. Then optimal codes were computed on these patches in similar fashion as described above for MNIST data set.

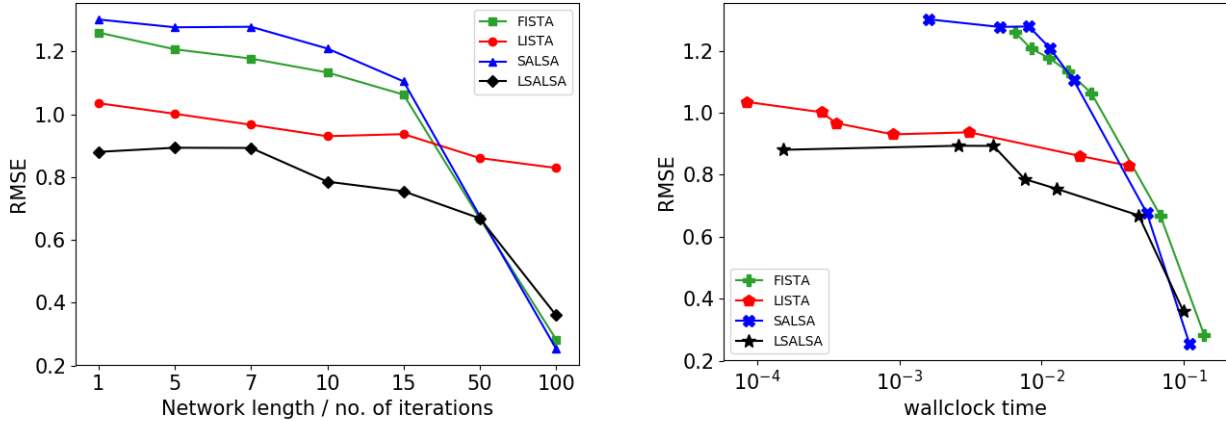


Figure 16: (a) CIFAR-10 code prediction errors for varying number of iterations. All methods except LISTA are converging fast after  $T = 50$  on this data set. LISTA, FISTA, and SALSAs took more than 15 iterations to produce error obtained by LSALSA in only 1 iteration. (b) CIFAR-10 code prediction error as a function of the wallclock time.

Iter	Classification Error (in %)			
	FISTA	LISTA	SALSAs	LSALSA
1	86.8600	79.1300	89.0700	<b>64.6900</b>
5	82.3300	76.2600	87.2700	<b>66.3100</b>
7	79.4700	74.1000	82.7100	<b>64.6400</b>
10	75.5200	71.6500	82.8300	<b>54.9800</b>
15	70.1900	72.4500	75.4100	<b>54.9900</b>
50	<b>43.1400</b>	66.3400	43.6100	49.4100
100	67.8600	60.2200	<b>10.4800</b>	18.4400

Table 6: CIFAR-10 classification results. The best performer is in bold.

## D. Additional MCA experiments

### D.1. MNIST + CIFAR

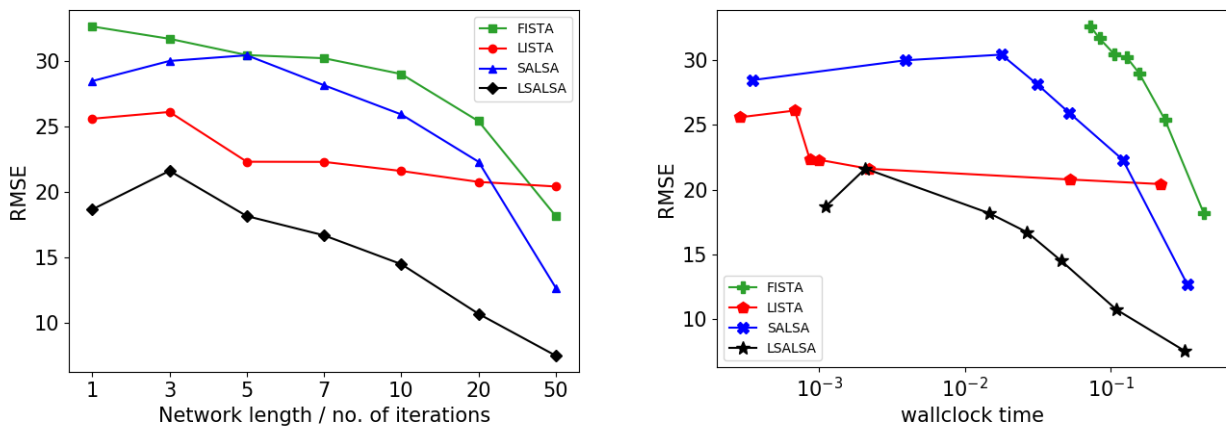


Figure 17: MCA experiments with MNIST + CIFAR data sets. (a) Code prediction errors for varying numbers of iterations. (b) Code prediction error as a function of the wallclock time.

MNIST + CIFAR-10 MCA experimental results are summarized here. We combined whole  $32 \times 32$  MNIST digits images with grayscale  $32 \times 32$  CIFAR-10 images and performed source separation on them. Code prediction error curves are presented with respect to the number of iterations  $T$  and wallclock time used to make prediction in Figure 17. The classification results are captured in Table 7 for MNIST codes and Table 8 for CIFAR-10 codes.

Iter	Classification Error (in %)			
	FISTA	LISTA	SALSA	LSALSA
1	66.8726	37.1971	33.3767	<b>5.8773</b>
3	90.0000	33.2179	60.7343	<b>7.3075</b>
5	90.0000	18.0357	19.2877	<b>4.2980</b>
7	90.0000	15.8905	8.8672	<b>3.2094</b>
10	90.0000	13.5879	5.3613	<b>3.2018</b>
20	8.4367	10.1961	2.8601	<b>4.6468</b>
50	21.2430	6.4679	12.9358	<b>2.9800</b>

Table 7: MNIST classification error after source separation. The best performer is highlighted in bold.

Iter	Classification Error (in %)			
	FISTA	LISTA	SALSA	LSALSA
1	88.1200	87.4300	<b>83.9500</b>	84.2700
3	88.7300	88.1500	84.4200	<b>82.5500</b>
5	88.6300	81.9900	82.5900	<b>74.8700</b>
7	88.4300	82.8500	81.1000	<b>68.2100</b>
10	88.8500	80.0800	79.0200	<b>63.9300</b>
20	81.3000	79.1600	76.2400	<b>57.5300</b>
50	70.4000	81.0900	74.7100	<b>52.6000</b>

Table 8: CIFAR-10 classification error after source separation. The best performer is highlighted in bold.

### E. Additional plots: MNIST+ASIRRA

Figure 18 shows an extended version of Figure 7. In Figure 19 we illustrate each method’s sparsity/accuracy trade-off on the MNIST test data set, while varying  $T$ . The LSALSA retains both the highest sparsity and accuracy levels, even for small  $T$ , from among all the methods.

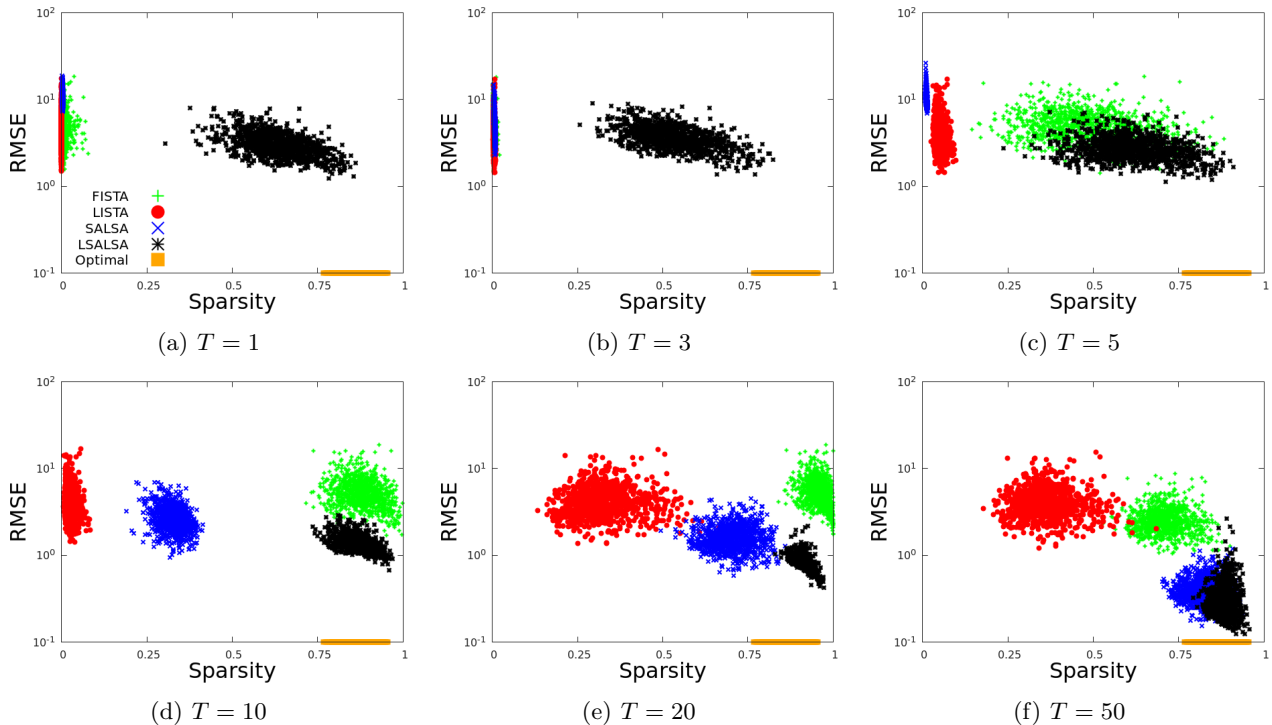


Figure 18: Sparsity/accuracy trade-off analysis for ASIRRA obtained for the source separation experiment with MNIST + ASIRRA data set. Each method corresponds to a colored point cloud, where each point corresponds to one sample from the ASIRRA test data set. LSALSA achieves the best sparsity/accuracy trade-off and is faster than other methods.

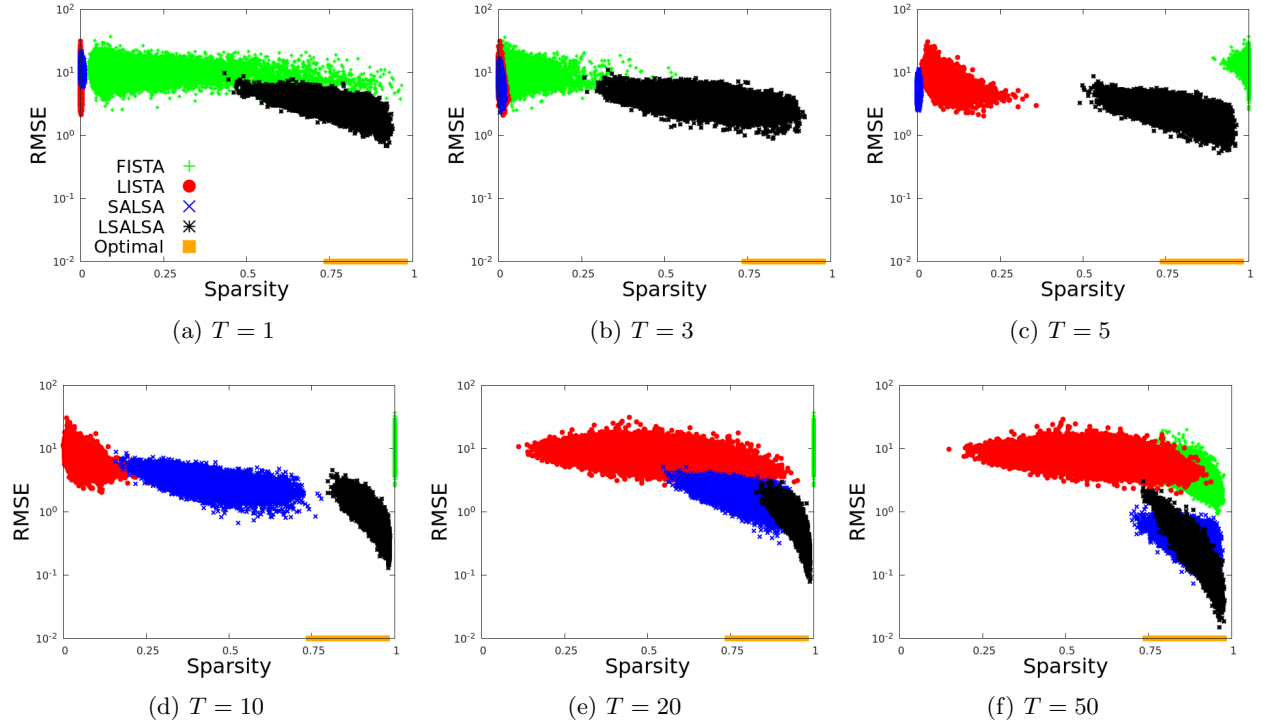


Figure 19: Sparsity/accuracy trade-off analysis for MNIST obtained for the source separation experiment with MNIST + ASIRRA data set. Each method corresponds to a colored point cloud, where each point corresponds to one sample from the ASIRRA test data set. LSALSA achieves the best sparsity/accuracy trade-off and is faster than other methods.

F. Source separation: image reconstruction results

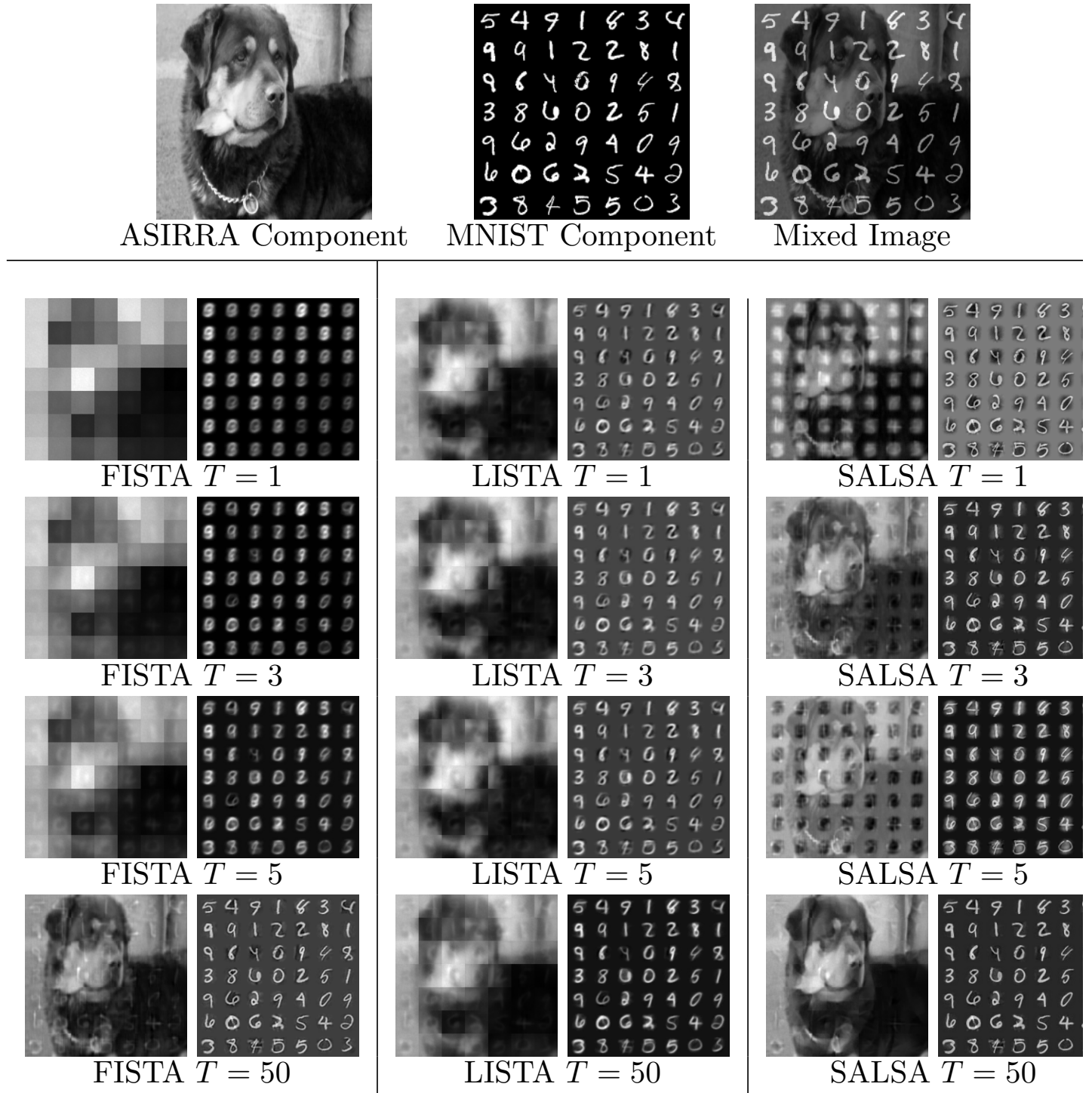


Figure 20: MCA experiment using MNIST + ASIRRA data set. Image reconstructions obtained by SALSA, LSALSA, FISTA, LISTA for  $T = 1, 3, 5, 50$ . Top row: original data (components and mixed).



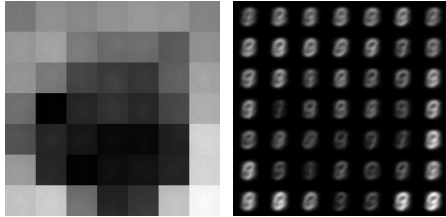
ASIRRA Component



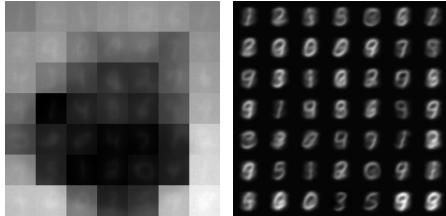
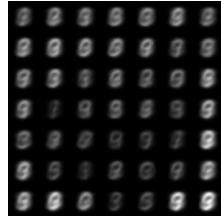
MNIST Component



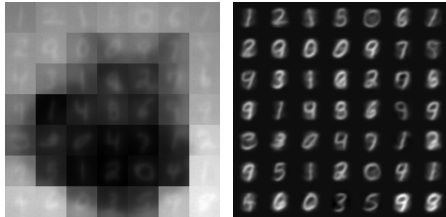
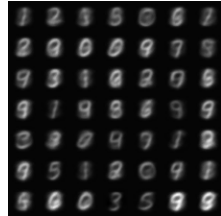
Mixed Image



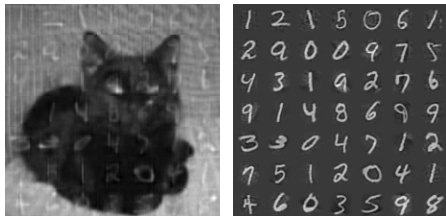
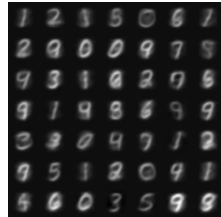
FISTA  $T = 1$



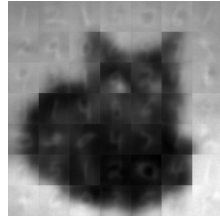
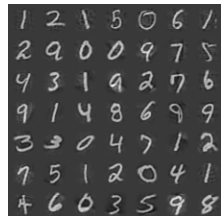
FISTA  $T = 3$



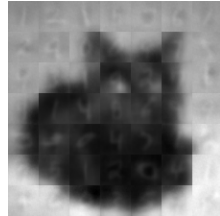
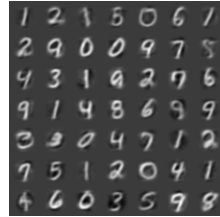
FISTA  $T = 5$



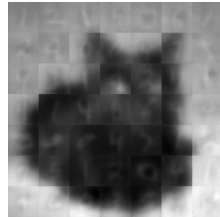
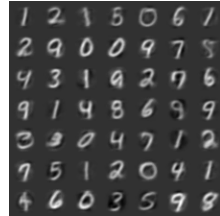
FISTA  $T = 50$



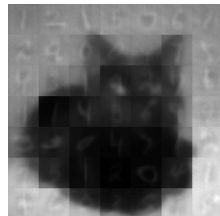
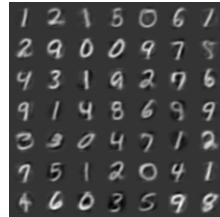
LISTA  $T = 1$



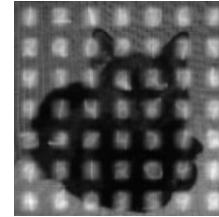
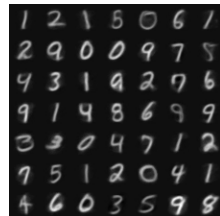
LISTA  $T = 3$



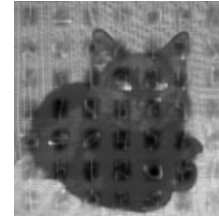
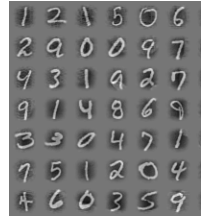
LISTA  $T = 5$



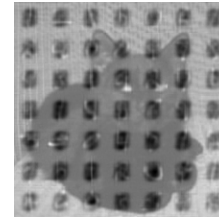
LISTA  $T = 50$



SALSA  $T = 1$



SALSA  $T = 3$



SALSA  $T = 5$



SALSA  $T = 50$



Figure 21: MCA experiment using MNIST + ASIRRA data set. Image reconstructions obtained by SALSA, LSALSA, FISTA, LISTA for  $T = 1, 3, 5, 50$ . Top row: original data (components and mixed).

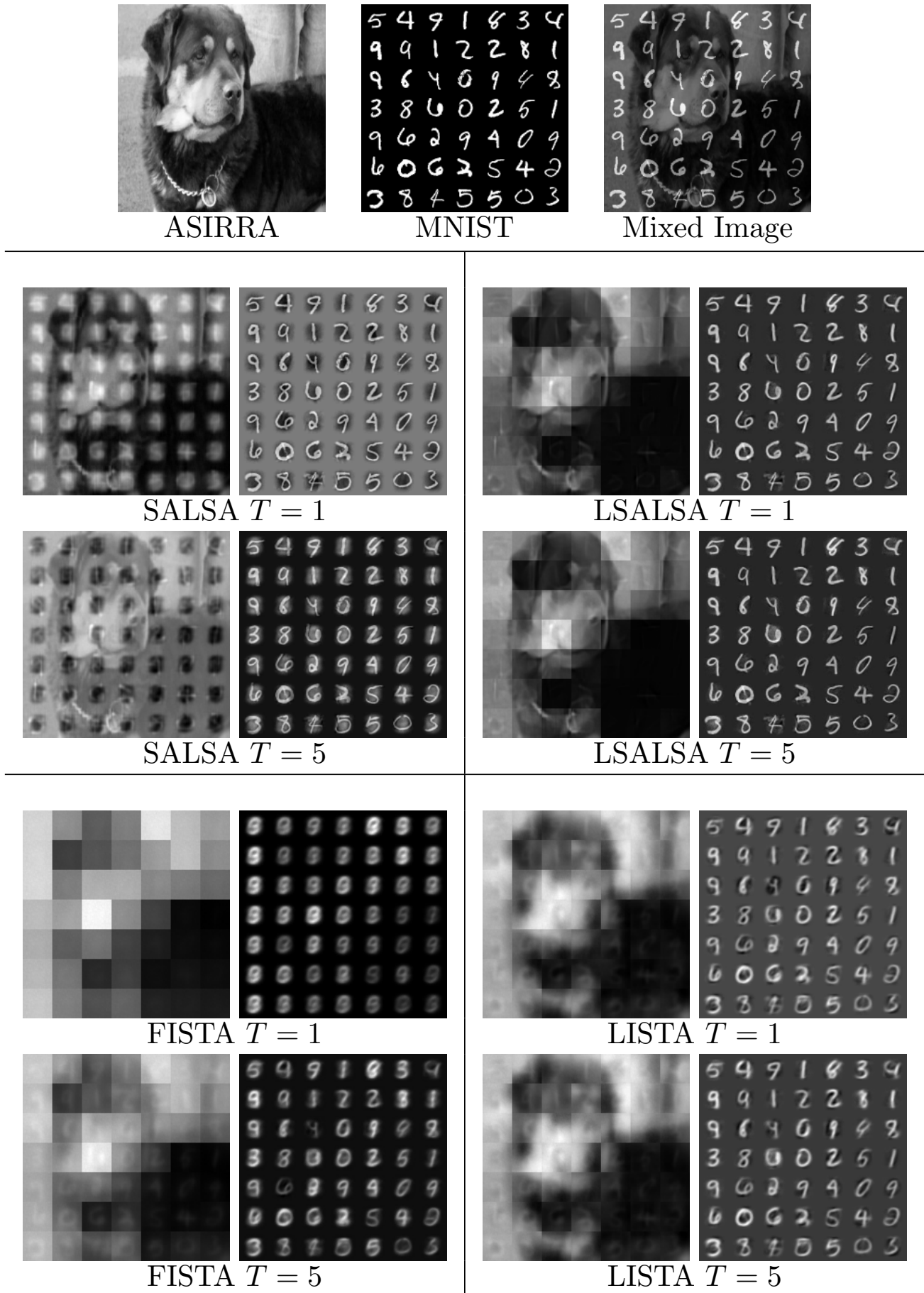
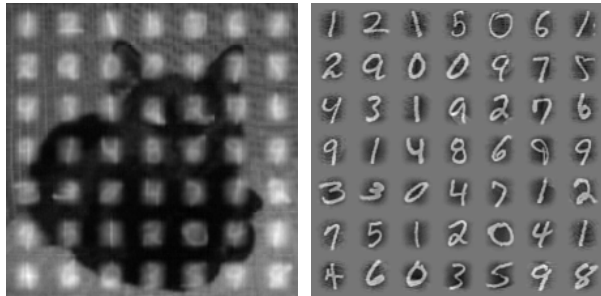
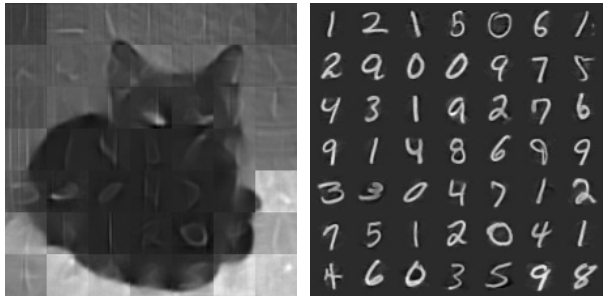


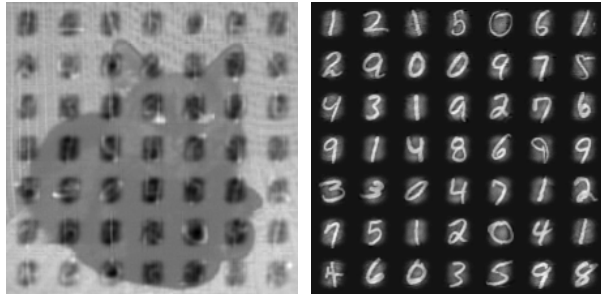
Figure 22: MCA experiment using MNIST + ASIRRA data set. Image reconstructions obtained by SALSA, LSALSA, FISTA, LISTA for  $T = 1, 5$ . Top row: original data (components and mixed).



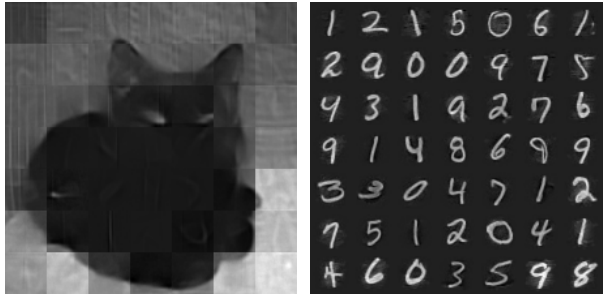
SALSA  $T = 1$



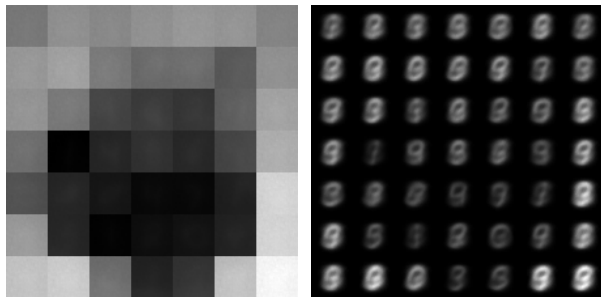
LSALSA  $T = 1$



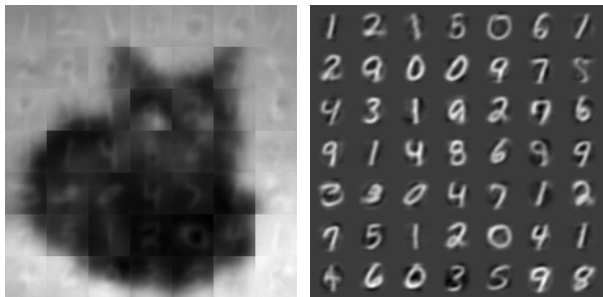
SALSA  $T = 5$



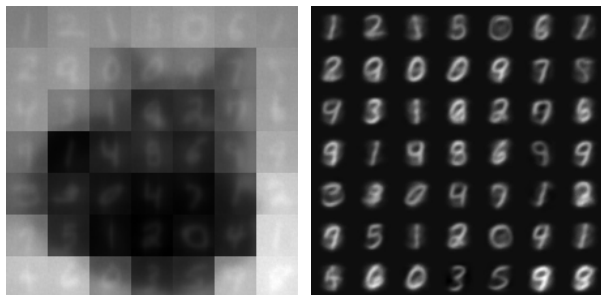
LSALSA  $T = 5$



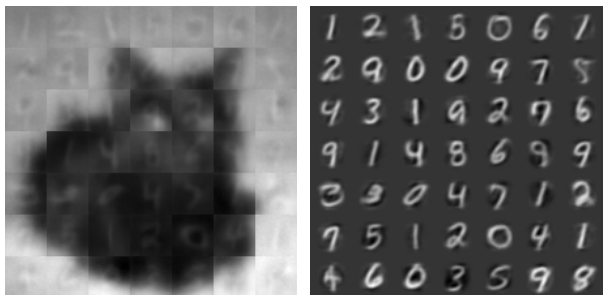
FISTA  $T = 1$



LISTA  $T = 1$

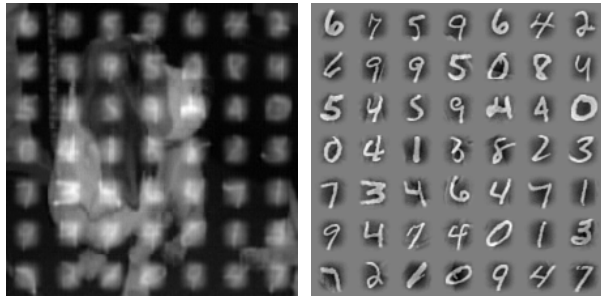


FISTA  $T = 5$

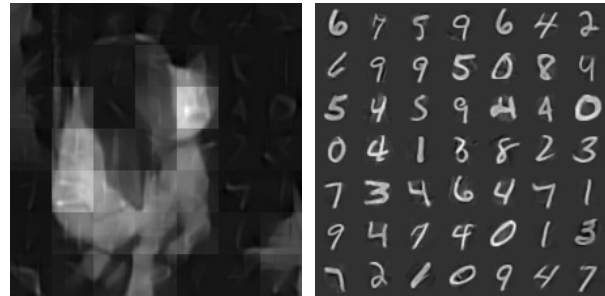


LISTA  $T = 5$

Figure 23: MCA experiment using MNIST + ASIRRA data set. Image reconstructions obtained by SALSA, LSALSA, FISTA, LISTA for  $T = 1, 5$ . Top row: original data (components and mixed).



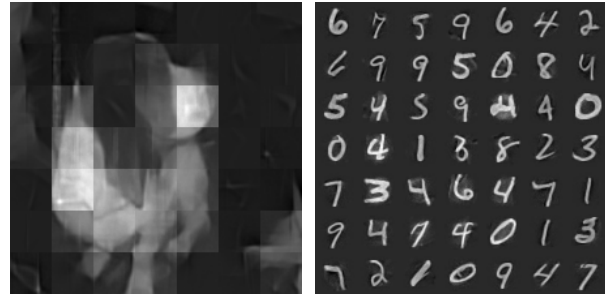
SALSA  $T = 1$



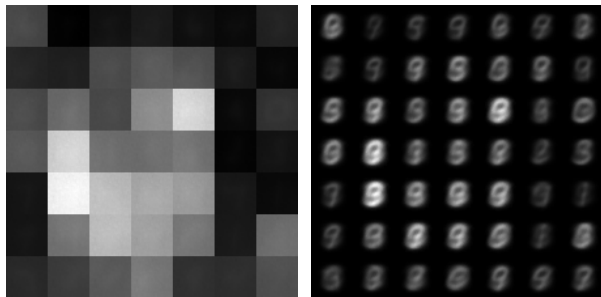
LSALSA  $T = 1$



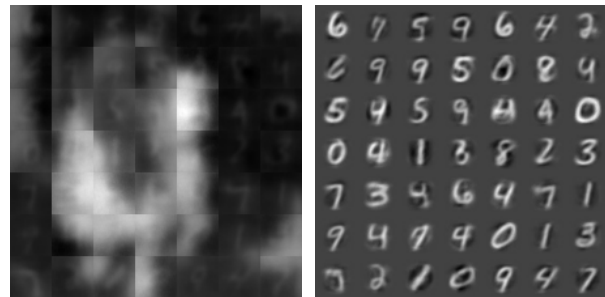
SALSA  $T = 5$



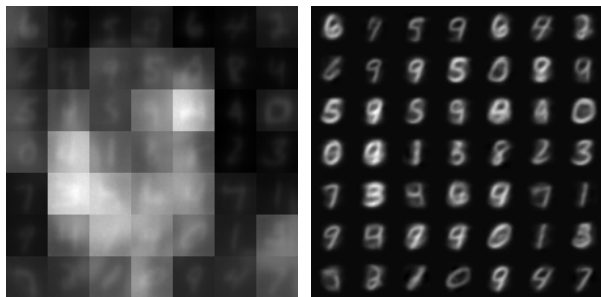
LSALSA  $T = 5$



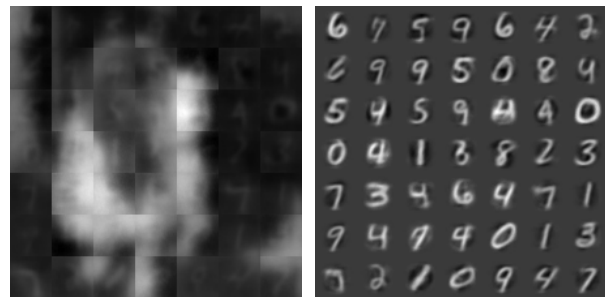
FISTA  $T = 1$



LISTA  $T = 1$



FISTA  $T = 5$



LISTA  $T = 5$

Figure 24: MCA experiment using MNIST + ASIRRA data set. Image reconstructions obtained by SALSA, LSALSA, FISTA, LISTA for  $T = 1, 5$ . Top row: original data (components and mixed).